Regd. No. C-3911

VOL. 34

INDIAN JOURNAL OF PHYSICS

No. 11

(Published in collaboration with the Indian Physical Society)

AND

VOL. 43

PROCEEDINGS

No. 11

OF THE

INDIAN ASSOCIATION FOR THE CULTIVATION OF SCIENCE

NOVEMBER 1960

PUBLISHED BY THE

INDIAN ASSOCIATION FOR THE CULTIVATION OF SCIENCE

JADAVPUR, CALCUTTA 32

Annual Subscription—
Inland Rs. 25.00
Foreign £ 2-10-0 or $ 7.00

NOTICE TO INTENDING AUTHORS

Manuscripts for publication should be sent to the Assistant Editor, Indian Journal of Physics, Jadavpur, Calcutta-32.

The manuscripts submitted must be type-written with double space on thick foolscap paper with sufficient margin on the left and at the top. The original copy, and not the carbon copy, should be submitted. Each paper must contain an Abstract at the beginning.

All References should be given in the text by quoting the surname of the author, followed by year of publication, *e.g.*, (Roy, 1958). The full Reference should be given in a list at the end, arranged alphabatically, as follows; Roy, S. B., 1958, *Ind. J. Phys.*, **32**, 323.

Line diagrams should be drawn on white Bristol board or tracing paper with black Indian ink, and letters and numbers inside the diagrams should be written neatly in capital type with Indian ink. The size of the diagrams submitted and the lettering inside should be large enough so that it is legible after reduction to one-third the original size. A simple style of lettering such as gothic, with its uniform line width and no serifs should be used, *e.g.*,

A·B·E·F·G·M·P·T·W·

Photographs submitted for publication should be printed on glossy paper with somewhat more contrast than that desired in the reproduction, and should, if possible, be mounted on thick white paper.

Captions to all figures should be typed in a separate sheet and attached at the end of the paper.

The mathematical expressions should be written carefully by hand. Care should be taken to distinguish between capital and small letters and superscripts and subscripts. Repetition of a complex expression should be avoid by representing it by a symbol. Greek letters and unusual symbols should be identified in the margin. Fractional exponents should be used instead of root signs.

IMPORTANT PUBLICATIONS

The following special publications of the Indian Association for the Cultivation of Science, Jadavpur, Calcutta, are available at the prices shown against each of them:—

TITLE	AUTHOR	PRICE
Magnetism ... Report of the Symposium on Magnetism		Rs. 7 0 0
Iron Ores of India	... Dr. M. S. Krishnan	5 0 0
Earthquakes in the Himalayan Region	... Dr. S. K. Banerji	3 0 0
Methods in Scientific Research	.. Sir E. J. Russell	0 6 0
The Origin of the Planets	.. Sir James H. Jeans	0 6 0
Active Nitrogen—A New Theory.	.. Prof. S. K. Mitra	2 8 0
Theory of Valency and the Structure of Chemical Compounds.	.. Prof. P. Ray	3 0 0
Petroleum Resources of India	.. D. N. Wadia	2 8 0
The Role of the Electrical Double-layer in the Electro-Chemistry of Colloids.	.. J. N. Mukherjee	1 12 0
The Earth's Magnetism and its Changes	.. Prof. S. Chapman	1 0 0
Distribution of Anthocyanins	.. Robert Robinson	1 4 0
Lapinone, A New Antimalarial	.. Louis F. Fieser	1 0 0
Catalysts in Polymerization Reactions	.. H. Mark	1 8 0
Constitutional Problems Concerning Vat Dyes.	.. Dr. K. Venkataraman	1 0 0
Non-Aqueous Titration	.. Santi R. Palit, Mihir Nath Das and G. R. Somayajulu	3 0 0
Garnets and their Role in Nature	.. Sir Lewis L. Fermor	2 8 0

A discount of 25% is allowed to Booksellers and Agents.

NOTICE

No claims will be allowed for copies of journal lost in the mail or otherwise unless such claims are received within 4 months of the date of issue.

RATES OF ADVERTISEMENTS

1. Ordinary pages:
   - Full page .. .. Rs. 50/- per insertion
   - Half page .. .. Rs. 28/- per insertion
2. Pages facing 1st inside cover, 2nd inside cover and first and last page of book matter:
   - Full page .. .. Rs. 55/- per insertion
   - Half page .. .. Rs. 30/- per insertion
3. Cover pages .. .. by negotiation

25% commissions are allowed to *bona fide* publicity agents securing orders for advertisements.

55

DAY TO DAY CHANGES IN THE DAILY MEAN INTENSITY OF COSMIC RAYS

R. P. KANE, S. R. KANE AND B. A. HOLLA

PHYSICAL RESEARCH LABORATORY, AHMEDABAD

(*Received, August* 12, 1960)

ABSTRACT. Data obtained at Kodaikanal (geomag. lat. 1°N, altitude 2300 meter) for cosmic ray mesons and the nucleonic component are analysed for the first 12 months of the I.G.Y. (July 1957–June 1958). Day to day changes of the mean intensity and their relationship with geomagnetic phenomena are studied. Comparison is made with neutron monitor data at Huancayo, Ottawa and Resolute. A variation spectrum of the type $\delta D(E)/D(E) \propto E^{-1}$ is obtained.

I. INTRODUCTION

During the I.G.Y. period, several workers in the world have operated cosmic ray meson telescopes and neutron monitors on a continuous basis. The Physical Research Laboratory, Ahmedabad, India, also participated in this effort and contributed data for neutron monitors and cubical meson telescopes for the stations at Ahmedabad and Kodaikanal. Besides these instruments, a narrow angle telescope of semi-angles 10° in the E–W plane and 20° in the N–S plane was also operated at Kodaikanal during the I.G.Y. period. Since meson telescopes and neutron monitors at different latitudes and altitudes have different energy responses to the primary cosmic ray intensity, a comparison of data from these gives an idea about the energy dependence of cosmic ray variations.

In this communication we have described the results of an analysis of results obtained with five different cosmic ray measuring instruments. Details of these are given in Table I.

TABLE I

Details of the stations

Instrument	Situation	Alt. (met.)	Geomagnetic		Cut off energies (BeV)
			Lat.	Long.	
Meson telescope ($10° \times 20°$)	Kodaikanal	2343	1°	147°	15
Neutron pile	Kodaikanal	2343	1°	147°	15
,,	Huancayo	3400	−1°	354°	13
,,	Ottawa	101	57°	351°	2
,,	Resolute	17	83°	289°	0

II. ENERGY RESPONSE OF THE VARIOUS INSTRUMENTS

Before proceeding with an examination of the results of analysis of the data from the various instruments, it is advisable to get an idea of the differences in their energy responses. This was attempted by following Dorman's (1957) method, which is outlined below :

The number N (h) of secondary cosmic ray particles at a latitude λ and at an atmospheric depth (h) is given by

$$N_\lambda(h) = \int_{E_\lambda^c}^{\infty} D(E).M(E, h)dE \qquad \ldots \quad (1)$$

where $D(E)$ represents the primary energy spectrum at the top of the atmosphere and $M(E, h)$ is the "multiplity function" which gives the number of secondary particles produced by a primary particle of energy E. The lower limit of integration E_λ^c is the minimum (critical) energy for arrival of primary cosmic rays in the vertical direction at latitude λ.

Dividing Eq. (1) by $N_\lambda(h)$ and multiplying by 100, we get

$$100\% = 100 \int_{E_\lambda^c}^{\infty} \frac{D(E)M(E, h)dE}{N_\lambda(h)} = \int_{E_\lambda^c}^{\infty} W(E, h)dE \qquad \ldots \quad (2)$$

where $W(E, h)$ represents the percentage contribution to the secondary component at depth h, due to primaries of energy E. $W(E, h)$ is known as the "coupling constant". A knowledge of its functional relationship with E is necessary to get an idea of the energy response of any particular instrument. W involves the product of the primary energy spectrum $D(E)$ and the multiplicity function $M(E, h)$. The primary energy spectrum of cosmic ray intensity is now fairly well established. But the multiplicity function $M(E, h)$ is difficult to calculate theoretically because of many complex processes involved in the interactions of primary cosmic ray particles with air nuclei. Dorman (1957) has pointed out that the coupling constants W can also be evaluated from a knowledge of the latitutde dependance of cosmic ray intensity, as follows :

Differentiating (1) partially with respect to E_λ^c, we get

$$\frac{\partial N_\lambda(h)}{N_\lambda(h)} = -\partial E_\lambda^c \frac{D(E) \, . \, M(E, h)}{N_\lambda(h)} = -\partial E_\lambda^c \, . \, W_\lambda(E, h) \qquad \ldots \quad (3)$$

It is clear, therefore, that $W(E, h)$ is directly related to the latitude effect of the secondary component observed at a depth h. Since the latitude effects of the

various secondary components have been precisely obtained experimentally, the coupling constants $W(E, h)$ can be easily calculated for energies between 0 and 15 BeV which is the maximum vertical cut-off energy (at $\lambda = 0$). For higher energies, Dorman suggests extrapolation methods which are based partly on experimental results and partly on theoretical considerations.

The coupling constants $W(E, h)$ are different for different secondary components and for different altitudes and latitudes and have been calculated by Dorman from experimental latitude effect data. Fig. 1 gives the coupling constants as percentage per BeV for the various secondary components mentioned in Table I. Since the latitude dependence of the meson component at the altitude of Kodaikanal is not known, the coupling constants for the same are obtained by averaging the coupling constants for Ion-chamber measurements at 10 Km altitude and hard component measurements at sea-level.

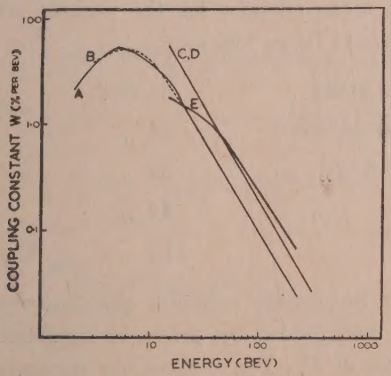

Fig. 1. Coupling constant W (percentage per BeV) for various secondary components. A-Resolute neutrons, B-Ottawa neutrons, C-Huancayo neutrons, D-Kodaikanal neutrons, E-Kodaikanal mesons. All plots are normalised to give $\int W.dE = 100$.

Knowing the value of W for all energies between E and ∞, it should be possible to calculate the mean energies to which the various instruments respond. A statistical method of obtaining the same would be to calculate mean energy $\bar{E}$ by the formula

$$\bar{E} = \frac{\int_{E_\lambda^c}^{\infty} W(E) \,.\, E \,.\, dE}{\int_{E_\lambda^c}^{\infty} W(E) \,.\, dE} \qquad \ldots \quad (4)$$

However, this method does not succeed for any of the curves given in Fig. 1 because of the following reason. For high emergies, the plots in Fig. 1 can be

approximated to a relation of the type $W = k.E^{-\nu}$. However, the values of ν are all less than 2 whereas the integral in the numerator of Eq. (4) is convergent only if $\nu > 2$. Hence, Eq. (4) does not yield finite values for the mean energy $\overline{E}$.

Fonger *et al.* (1953) have avoided this difficulty by assuming an arbitrary definition of mean energy $\overline{E}$ as,

$$\frac{1}{1+\overline{E}} = \frac{\int_{E_\lambda^c}^{\infty} \frac{W(E) \cdot dE}{1+E}}{\int_{E_\lambda^c}^{\infty} W(E)dE} \qquad \ldots (5)$$

Using this formula, the mean energies for the various secondary components referred to in Table I would be as follows:

Kodaikanal meson		54 BeV
Kodaikanal neutron		34 „
Huancayo	„	34 „
Ottawa	„	12 „
Resolute	„	11.5 „

One may also view the energy response qualitatively by calculating the percentage of particles contributed by primaries confined to an energy range 0 to E for various values of E. Fig. 2 gives the percentages for the various secondary components.

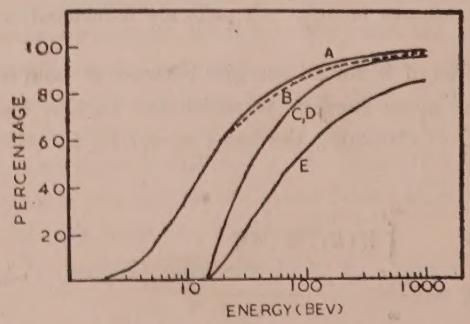

Fig. 2. Percentage of secondary particles contributed by primaries of energies below E. Symbols A, B, C, D & E have the same meaning as in Fig. 1.

It can be seen from Fig. 2 that for the neutron monitors at Ottawa and Resolute, almost 50% of the secondaries are due to primary energies between

0 to 15 BeV while for the nucleonic component at Huancayo and Kodaikanal the corresponding energy range is 15 to 35 BeV. For Kodaikanal meson intensity, the range is still higher viz. 15 to 75 BeV.

III. DAILY MEAN INTENSITY OF COSMIC RAYS

The daily mean intensities of the nucleonic component and meson component of cosmic ray intensity at the various places corrected for barometric effect only are plotted in Fig. 3 for the period July 1957 to June 1958. The daily means of H, the horizontal component of earths magnetic field at Kodaikanal, are also plotted.

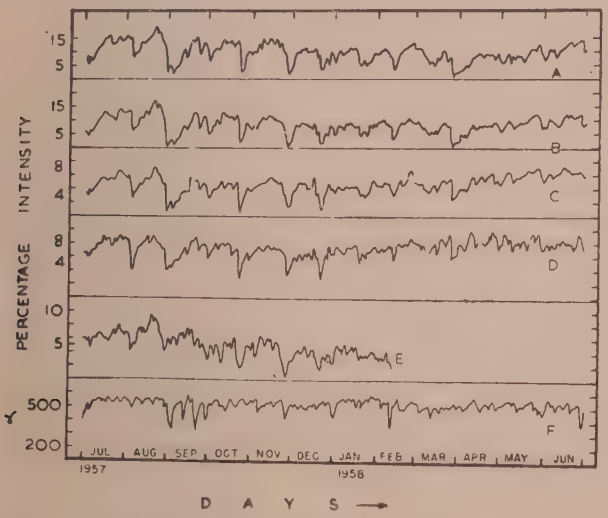

Fig. 3. Plot of daily mean intensities. Symbols A, B, C, D, E are as in Fig. 1. H represents the horizontal component of earths magnetic field at Kodaikanal..

It can be seen from Fig. 3 that the daily mean intensity shows large fluctuations during the period under consideration. Variations as high as 5% at the equatorial stations and 10% or more at high latitude stations are observed frequently. Many of the sharp minima indicate Forbush type decreases.

To find out the extent to which these variations are simultaneous at the various stations, correlation coefficients are calculated for the various pairs. They are given in Table II.

It can be seen from Table II that

(a) Kodaikanal neutrons and Huancayo neutrons are very highly correlated with each other but not so much with either Kodaikanal mesons or Ottawa and Resolute neutrons.

TABLE II

Correlation coefficients between the various components

	Kodaikanal meson	Kodaikanal neutron	Huancayo neutron	Ottawa neutron	Resolute neutron
Kodaikanal meson	1.00	0.68	0.70	0.70	0.59
Kodaikanal neutron	0.68	1.00	0.91	0.73	0.66
Huancayo neutron	0.70	0.91	1.00	0.86	0.71
Ottawa neutron	0.70	0.73	0.86	1.00	0.97
Resolute neutron	0.59	0.66	0.71	0.97	1.00

(b) Ottawa and Resolute neutrons are very highly correlated with each other.

It seems, therefore, that the mean intensity variations are broadly parallel at all the stations indicating a world wide nature of the variations, but there are differences also between stations at different latitudes as also between mesons and nucleonic component. It is also observed that the average ranges of the variations for Kodaikanal neutron and Huancayo neutron are about the same, while the ranges of neutron intensity at Ottawa and Resolute are more than twicet hose at Kodaikanal or Huancayo. Kodaikanal meson intensity has a range somewhat lesser than Kodaikanal neutron intensity. This indicates a strong energy dependence where lower energies have larger variations.

It must be noted, however, that the meson intensity is not corrected for upper air temperature effect and is not, therefore, directly comparable to the neutron intensities. The lower correlation between neutron and meson intensities could be due to this fact. Unfortunately, upper air radio-sonde data for Kodaikanal are not available and hence it is not possible to estimate and correct for the upper air temperature effect at Kodaikanal.

IV. RECURRENCE TENDENCIES IN THE DAILY MEAN INTENSITY VARIATIONS

To study the recurrence tendencies in the daily mean intensity, the days on which Ottawa neutron intensity showed maxima and minima were chosen as epoch days and Chree diagrams were drawn for the various intensities for $n = -60$ to $+60$ about the epoch day $n = 0$. These are shown in Fig. 4.

Fig. 4(a) and 4(b) refer to Ottawa neutron intensity maxima and minima respectively as epochs. It will be seen that there is a 27-day recurrence tendency for both the maxima and minima. Chree diagram for H, the horizontal component of earths magnetic field at Kodaikanal is also plotted in Fig. 4. It will be seen from Fig. 4(b) that H has a minimum at $n = 0$ which means that on cosmic ray minima days, value of H is also minimum. However, the magnitude of the minimum in H is rather small ($\sim$70 gamma). This is discussed further in Sectuoı V.

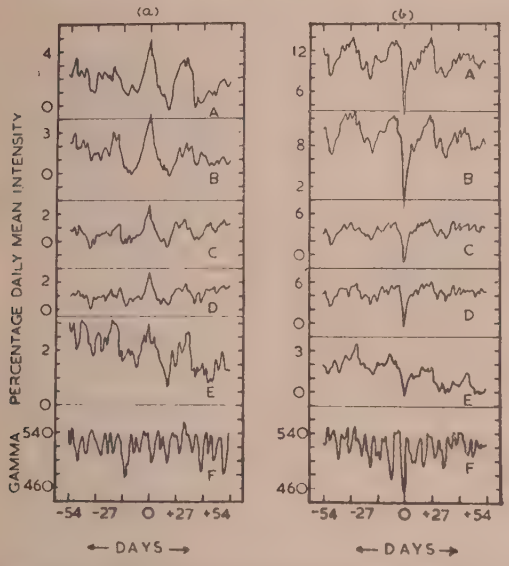

Fig. 4. Chree diagrams of daily mean intensities of cosmic rays and earth's magnetic field for Ottawa neutron intensity (a) Maxima and (b) Minima as epoch days.
A-Ottawa neutron, B-Resolute neutron, C-Huancayo neutron, D-Kodaikanal neutron, E = Kodaikanal meson, F = Horizontal component of earths magnetic field.

V. RELATIONSHIP WITH GEOMAGNETIC DISTURBANCES

As a measure of the geomagnetic disturbance of any particular day, a character figure C_p is evolved, which takes into account deviations from averages of the

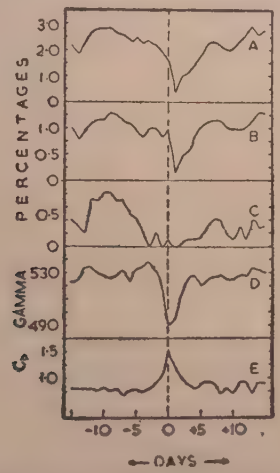

Fig. 5. Chree diagrams of daily mean intensities of cosmic rays and earths magnetic field for C_p maxima as epoch days. A-High latitude neutrons, B-Equator neutrons, C-Equator mesons, D-Horizontal component of earths magnetic field, E-C_p values.

variations in the various magnetic elements at several locations all round the world. Values of C_p range from 0 to about 2.0 To study the relationship between C_p and cosmic ray variations, days of maxima of C_p values were chosen as epoch days and Chree diagrams were drawn for the daily mean intensity of cosmic rays. These are shown in Fig. 5.

It seems that C_p maxima are followed within a day or two by cosmic ray minima. This is in agreement with earlier observations of similar nature by workers elsewhere (e.g. Simpson 1954).

However, it is found that the changes in the mean cosmic ray intensity associated with C_p maxima are not very large. Thus, the changes at equator are of the order of 1% only whereas it is seen from Fig. 1, that the mean intensity variations are sometimes as large as 5% for equatorial stations. It is obvious, therefore, that there is no one-to-one relationship between C_p maxima and cosmic ray minima. Apart from the possibility that some of the cosmic ray changes have apparently no connection with C_p maxima at all, it is also possible that all C_p maxima are not on the same footing so far as their effects on cosmic ray intensity are concerned. It is worthwhile, therefore, to see whether a criterian could be decided, upon which one could separate out those C_p maxima which are better related to cosmic ray changes than the others. In the past, attempts have been made (Sekido *et al.*, 1955) to study separately cosmic ray storms which are, and are not, associated with geomagnetic disturbances. However, the selection criterion there is the effect on cosmic ray intensity itself. We have adopted a criterion which was first introduced by Allen (1944). The C_p maxima are divided into 4 groups accaccording to whether they are preceded and/or succeeded by significant maxima at 27 day interval. Thus, the four groups are :—

Group A: $^{+}C_p^{+}$ C_p maxima preceded and succeeded by C_p maxima at ± 27 days.

Group B: $^{\circ}C_p^{+}$ C_p maxima succeeded by C_p maxima at $+27$ days but not preceded at -27 days.

Group C: $^{+}C_p^{\circ}$ C_p maxima preceded by C_p maxima at -27 days but not succeeded at $+27$ days.

Group D: $^{\circ}C_p^{\circ}$ C_p maxima having no preceding or succeeding maxima at ± 27 days.

Taking C_p maxima in each group separately as epoch days, Chree diagrams were drawn for the various cosmic ray intensities as also for the horizontal component of earths magnetic field. In Table III, we have summarised the main features of the Chree diagrams. For comparison, the main features as revealed by Fig. 5 for all C_p maxima as epochs are also included in Table III.

It is clearly seen from Table III that though all types of C_p maxima produce cosmic ray minima at about $n = 0$ to $+2$, the magnitude of the drop in cosmic

TABLE III

Repationship between Cp maxima and cosmic ray intensity

Epoch days ($n = 0$)	Range of Cp	Cosmic ray minima at	Magnitude of cosmic ray intensity drop			Ratio of range high lat : equator (neutrons)	Horizontal component of magnetic field at Kodaikanal		
			Equator		High lat.		Min. at	Intensity drop	Remarks
			Meson	Neutron	Neutron				
All C_p max.	About 0.5 to 1.5	$n = +1$ day	0.5%	1.0%	2.0%	2.0	$n = 0$	45 gamma	Maximum at $n = 0$ very prominent.
$^{+}C_p^{+}$ max.	,,	About $n = +1$	0.5%	0.5%	1.5%	3.0	About $n = +1$	40 gamma	Large fluctuation of H values on days on either side of $n = 0$.
$^{\circ}C_p^{-}$ max.	,,	,,	0.5%	0.5%	1.5%	3.0	$n = 0$	55 gamma	,,
$^{+}C_p^{\circ}$ max.	,,	,,	1.2%	1.5%	3.0%	2.0	$n = +1$	60 gamma	,,
$^{\circ}C_p^{\circ}$ max.	,,	,,	1.2%	1.5%	4.5%	3.0	$n = 0$	70 gamma	Effect at $n = 0$ very prominent.

ray intensity is not the same for all. Thus, ${}^{+}Cp^{0}$ and ${}^{0}Cp^{0}$ maxima which are characterised by either a fading or an absent recurring tendency have the largest effect on cosmic rays. The effect is about 1.5% at equator and 4% at high latitude for neutrons. The ratio of these two is, however, about the same for all types of C_p maxima.

It seems, therefore, that C_p maxima which do not have recurring tendencies produce the greatest reduction in cosmic ray intensity. From the last two columns of Table III, it is seen that the association of all C_p maxima with characteristics of H variation is not the same. Thus the C_p maxima of the ${}^{+}C_p{}^{0}$ or ${}^{0}C_p{}^{0}$ type show a larger range in the value of H as compared to the range due to other C_p maxima.

It is now well-known that geomagnetic disturbances of the recurring type are associated with coronal activity and C.M.P. of weak coronal emission. On the other hand, the non-recurring type disturbances are associated with S. C. type of magnetic storms and also with sunspot groups of complex magnetic field, and with C.M.P. of sunspot groups having high activity in solar radio noise. It seems, therefore, that cosmic ray events have a better association with phenomena of the latter type.

There are, however, two major apparent discrepancies in these observations. They are as follows :

(a) Through C_p maxima having little or no 27 day recurrence tendencies are better associated with cosmic ray minima, the Chree diagrams for cosmic ray intensity minima as epochs show prominent recurrence tendencies as shown in Fig. 4(b).

(b) Though the non-recurring type C_p maxima are also associated with S. C. type magnetic storms, there is no one-to-one relationship between cosmic ray storms (viz. sharp minima of cosmic ray intensity) and the S.C. type storm decreases of the horizontal component of earths magnetic field.

These discrepancies can, however, be understood if the following assumptions are made:

(i) The recurring type geomagnetic disturvances do have some effect on cosmic ray intensity though the effects are not so prominent as in the case of effects of non-recurrent type storms. This is borne out by results given in Table III.

(ii) The non-recurring type disturbance need not be assumed to be directly responsible for cosmic ray minima but both may have a common source of origin. The effects of the common source may persist longer in cosmic ray intensity than in geomagnetic disturbances.

(iii) As stated earlier, all cosmic ray intensity minima are not associated with minima of horizontal component of earth's magnetic field. However, when a Chree diagram is drawn for intensity minima of the horizontal component of magnetic field at Kodaikanal as epoch days, it is found that the cosmic ray intensity shows a prominent minimum on or about the epoch days and the magnitude of this minima is quite large, about half of the general range of variation in cosmic ray intensity (Fig. 6). Thus, all cosmic ray storms are not associated with magnetic storms of the S.C. type. But many of the S.C. type magnetic storms are associated with cosmic ray storms. This is not incompatible with (a) and (b) above.

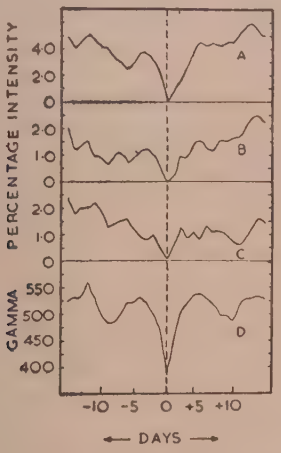

Fig. 6. Chree diagrams of daily mean intensities of cosmic rays for minima of horizontal component of earth's magnetic field as epoch days. A-High latitude neutrons, B-Equator neutrons, C-Equator mesons, D-Horizontal component of earth's magnetic field.

VI. ENERGY DEPENDENCE OF THE VARIATIONS IN PRIMARY INTENSITY

As has been shown so far, fluctuations as high as 5% at equator and 10-15% at high latitudes are observed in cosmic ray intensity. It is obvious, therefore, that the variations of cosmic ray intensity have energy spectra significantly different from the primary energy spectrum. Referring to Eq. (1), we obtain by differenciating partially with respect to $D(E)$,

$$100 \cdot \frac{\partial N_\lambda(h)}{N_\lambda(h)} = \int_{E_\lambda^0}^{\infty} \frac{\partial D(E)}{D(E)} \cdot W_\lambda(E, h) dE \quad \ldots (6)$$

For the L.H.S., the experimental values are about 3—4% for Kodaikanal mesons, about 5% for Kodaikanal and Huancayo neutrons and about 10-15% for Ottawa and Resolute neutrons.

It is found that a variation spectrum of the type $\partial D(E)/D(E) \propto E^{-1}$ fits the experimental values reasonably well.

It should be noted, however, that such a spectrum fits only to the gross effects mentioned above. In individual events and for smaller time intervals, far too large effects (100% or more) have been observed at high latitudes. The energy spectrum involved there should be far more steep. Values as high as E^{-5} have been suggested (Sekido and Murakami, 1955).

VII. CONCLUSION

The broad conclusions of the above analysis may be summarised as follows

(1) The daily mean intensities of cosmic rays as observed by meson telescope and neutron monitors at the stations of Kodaikanal, Huancayo, Ottawa and Resolute show large fluctuations during the period July 1957 to June 1958. The range of fluctuations is about 3—5% and 5% for mesons and neutrons respectively at equatorial stations and 10—15% for neutrons at high latitudes.

(2) The maxima and minima of the daily mean intensity of cosmic rays exhibit strong 27-day recurrence tendencies.

(3) An analysis with *Cp* maxima as epochs indicates that *Cp* maxima are followed by cosmic ray minima with a probable lag of 1 or 2 days. Amongst the *Cp* maxima, the non-recurrent types seem to be better associated with cosmic ray minima.

(4) Cosmic ray storms are not invariably associated with magnetic storms but magnetic storms of the S.C. type are many times associated with cosmic ray minima.

(5) Large cosmic ray intensity decreases are world-wide in nature but their magnitude seems to be more than double at high latitudes as compared to that at equator.

(6) The day to day variations of cosmic ray intensity are energy dependent. The variation spectrum $\partial D(E)/D(E)$ is of the type E^{-1} where $D(E)$ is the primary energy spectrum.

ACKNOWLEDGMENTS

The authors are grateful to Professor V. A. Sarabhai for valuable guidance during the course of this investigation. Thanks are due to various research groups who have contributed neutron monitor data during the I.G.Y. The co-operation of the staff of the Solar Physics Observatory Kodaikanal, is greatly appreciated.

Thanks are due to S. R. Thakore and others for computational help and to the Atomic Energy Commission of India for financial assistance.

REFERENCES

Allen, 1944, *Month. Notices of Roy. Astro. Soc.*, **104**. 13.

Dorman, I. L., 1957, "Cosmic Ray Variations" published by State Publishing House for Technical & Theoretical Literature, Moscow.

Fonger, W. H., 1953, *Phys. Rev.*, **91**, 351.

Sekido, Y., Wada, M., Kondo, I. and Kawabata, K., 1955, *Rep. Ionosph. Res. Japan.*, **2**, 174.

Sekido, Y. and Murakami, K., 1955, Proc. IUPAP Cosmic Ray Congress, Mexico. 253.

Simpson, J. A., 1954, *Phys. Rev.*, **94**, 426.

APPENDIX

Epoch dates for the various Chree diagrams

Month	Ottawa maxima	Ottawa minima	$^{+}C_p^{+}$ max.	$^{\circ}C_p^{+}$ max.	$^{+}C_p^{\circ}$ max.	$^{\circ}C_p^{+\circ}$ max.	H minima
Jul. 57	27					19	
Aug.	21	5,30		3,6	29	13	
Sep.	20	3,14	2	23	29	4,13	5,13,
		23,30					23,30
Oct.	10	23		14	21		
Nov.	13	27	9,18	7		26	27
Dec.	6,16,28	22	6		11,31	1	31
Jan. 58	10	18	21			18	
Feb.	5,23	12		6,21	17	11	11
Mar.	20	15,26			5,19	12,25	
Apr.	25	30	3,29	17			
May	26	31	14,26			29,31	
Jun.				7			

AN X-RAY STUDY OF SILVER-CADMIUM ALLOYS*

MD. ABDUL QUADER

Department of General Physics and X-rays,
Indian Association for the Cultivation of Science, Calcutta-32

(*Received, August* 24, 1960)

ABSTRACT. An X-ray investigation of the silver-cadmium system of alloys has been carried out to determine the phase boundaries at temperatures below 300°C with particular attention to the β-field. The presence of the β' phase, which occurs in the β-field at temperatures below 228°C has been confirmed. The lattice parameter and structure of the α, β' and ζ phases have been determined. An approximate boundary of the β' phase has been obtained. The boundaries of the other phases as obtained by us agree with those of Owen *et al.* The results are discussed in the light of the Hume-Rothery rule and the zone-theory.

INTRODUCTION

The equilibrium diagram of the silver-cadmium system of alloys, published in Metals Handbook (1948) is based on the thermal and microscopical work of Durrant (1931, 1935). In this diagram a phase β' (ordered body-centred cubic with CsCl type of structure) is given in the β-field. The diagram presented by Owen *et al.* (1939) from the X-ray investigation of the system differs from that given in Metals Handbook in respect of the exact position of the phase boundaries, though the arrangement of the different phases is similar. They, however, could not get the β'-phase at the lower temperature as their samples, according to them, could not be brought to a satisfactory state of equilibrium by annealing within a reasonable time.

The earlier X-ray investigations of the alloys by Astrand and Westgren (1928) and Natta and Freri (1928) revealed only the β and ζ phases. The only evidence of the β' phase from the X-ray study was given by Kosolapov and Trapeznikov (1936) who studied a single 51 atomic percent cadmium alloy in a high temperature camera and got the β' phase at 270°C and ζ phase at 500°C. Later work (Owen *et al.*), however, proved that the temperatures recorded by them were incorrect. Thus at present there is no satisfactory confirmation of the boundaries of the β' phase by *X*-ray methods. In the present work an attempt has been made to determine the phase boundaries of the silver-cadmium alloys at temperatures below 300°C with particular attention to the β-field where the β' phase occurs. The ζ to β' transformation was studied in detail by taking X-ray

*Communicated by Prof. B. N. Srivastava.

powder diffraction photographs of the alloys in the high temperature camera and also by taking photographs of quenched specimens of the alloys.

EXPERIMENTAL PROCEDURE

X-rays are intensively used to study the equilibrium diagram of metallic systems and are extremely valuable for the identification of phases in alloys. They may be used for this purpose even when it is not possible to index the diffraction lines or to solve the crystal structure. There are two general ways of applying X-rays to study the equilibrium diagrams : (a) the lattice parameter method and (b) the method of vanishing lines.

(a) *The lattice parameter method* :

In general the lattice parameter of pure metals changes, either decreases or increases, with the addition of a second metal i.e. on alloying. If the system does not form a continuous range of solid solutions, a break will occur in the lattice parameter composition curve, from which the limit of solid solubility can be determined. In the same way the limit of other intermediate phases, if any, can be established. Thus by applying this lattice parameter method the interphase boundaries between two phases, when they occur due to the change in composition, can be determined at any temperature.

(*b*) *The method of vanishing lines* :

If a standard film of a particular phase has been obtained, a simple visual examination of X-ray films is often sufficient to establish the existence of that particular phase in a polyphase alloy. The boundaries of the phase fields are determined by a method of X-ray bracketing, in which, if the diffraction lines due to a phase are present on one film and absent in another, the boundary is drawn between the temperatures or compositions to which the two films refer. The sensitivity of this method, however, depends on the width of the two-phase region and also whether the phases give rise to strong diffraction lines which do not overlap. In a favourable case as little as 1% of a given phase can be determined visually on a Debye-Scherrer film.

PREPARATION OF ALLOYS

Small amounts of silver-cadmium alloys up to 68 per cent by weight of cadmium where prepared from spectroscopically pure metals obtained from Johnson Matthey & Co., London. Accurately weighed quantities of silver and cadmium in the form of turnings (cleaned and dried) were taken in pyrex tubes, evacuated and sealed under very low pressure of helium, and heated in an electric furnace. The mixture was first heated for an hour at 500°C, when cadmium melted and got absorbed in silver by diffusion thereby lowering the melting point of silver. The temperature of the furnace was then raised till the alloy melted, when it was made

homogeneous by shaking and quenched in water to prevent segregation and inhomogeneity which might occur during slow cooling.

The prepared alloys were weighed to ensure that no loss had occurred during heating. The alloys were again sealed in evacuated pyrex tubes and homogenized at 600°C for 24 hours and then examined for homogeneity by taking filings from different parts of the lump. From the homogeneous lumps, powdered samples were prepared and taken in small pyrex tubes, evacuated and sealed. The tubes were suspended by means of a fine copper wire in a vertical tube furnace and annealed at different temperatures. The tubes could be dropped into cold water placed just below the furnace by opening the bottom door and cutting the suspension. The method yielded very efficient quenching. Specimen for the high temperature camera was prepared by taking the powder in thin-walled pyrex capillaries.

APPARATUS

Philips precision cameras with 57.3 and 114.5 mm diameter were used to take the powder photograph of the quenched alloys. High temperature X-ray photographs were taken in Unicam 19 cm high temperature camera, which was calibrated by measuring the lattice spacing of pure silver up to 500°C. CuK_α radiations from a sealed off Philips X-ray tube were used to obtain the diffraction photographs.

EXPERIMENTAL RESULTS

Powders of the silver-cadmium alloys situated within the range of composition from 47 to 58% by weight of cadmium were quenched from different temperatures and X-ray pictures were taken. A preliminary survey shows that this region contained a single body-centred cubic β' (ordered) phase below about 228°C bordered on either side by double phase regions. The alloy 47* is in $(\alpha+\beta')$ field below 228°C and in $(\alpha+\zeta)$ above it (See Fig.1). Both the alloys 56.4 and 58 are mixtures of β' ond γ, a complex body-centred cubic with 52 atoms per unit cell, below 220°C, above which they are in $(\zeta+\gamma)$ region. All the four alloys included between 50.8 to 53% by weight of cadmium are in the β'-field below about 228°C, and in the ζ phase above it. A second transformation from ζ to β (body-centred cubic with same lattice parameter as that of β') was also observed with these alloys. Thus when 51.57 alloy was quenched from 450°C it yielded β phase. The β phase was also obtained with 51.3 alloy when an exposure was given at 440°C in the high temperature camera. According to Owen this transformation occurs at 427°C for the alloys with compositions from 43.7 to 50% by weight of cadmium, and 445°C for the alloys from 56 to 60% cadmium. No attempt has been made here to redetermine this transformation

*Alloy 47 indicates an alloy with 47% by weight of cadmium.

temperature, but the observation on the two alloys mentioned above, confirmed their results.

(i) *The $\alpha/(\alpha+\beta')$ and $\alpha/(\alpha+\zeta)$ phase boundaries.*

Three α phase alloys with 25.1, 30.1 and 34.7% by weight of cadmium were prepared. In order to get a relation between lattice parameter and composition in the α phase, the lattice parameter of these alloys were measured. Powders of alloy 47 were annealed at 235°C for five days and quenched in water and X-ray powder photograph was taken. Sharp lines of α and ζ phases were obtained. The lattice parameter of α phase was calculated from (511) lines and those of ζ were obtained from $(21\bar{3}3)$, $(30\bar{3}2)$ and (0006) lines (the wave length used for CuK_α radiations are $CuK_{\alpha_1} = 1.54051$ and $K_{\alpha_2} = 1.54433$ Å). The alloy was again quenched from 224°C after annealing for five days, which yielded α and β' lines, from which the lattice parameters for α and β' phases were calculated. The results are given in the Table I. The α phase in the 47% alloy corresponds to 43.5 and 43.4% by weight of cadmium at 235 and 224°C respectively, as obtained by extrapolating the lattice parameter composition curve for α phase alloys. These gave the limit of the α phase. By narrowing the limits of annealing temperatures a temperature of 228°C$\pm$1 was obtained for this alloy at which $\beta'-\zeta$ transformation occurs.

TABLE I

Lattice parameter of α-phase alloys

Alloy composition in wt. % of Cd.	Lattice parameter at 30°C in Å	Quenching temperature °C
25.1	4.1400	—
30.1	4.1518	—
34.7	4.1635	—
47.0	4.1839	235
47.0	4.1837	224
47.0	4.1835	180

(ii) *The $(\alpha+\zeta)/\zeta$ and $(\alpha+\beta')/\beta'$ phase boundaries*

The four alloys included between 50.8 and 53% cadmium by weight are all in the β' field below the transformation temperature and in the ζ phase above it. Alloy 51.3 was studied in the high temperature camera up to 440°C. The photograph taken at 440°C shows that the alloy again changed to body-centred cubic phase.

The $\beta'-\zeta$ transformation was studied in detail for the 51.3 alloy using the high temperature camera. For that purpose exposures in the high temperature camera were made at several temperatures between 220 to 240°C. A temperature hysteresis was observed in course of taking these photographs. Thus it has been observed that β' transforms to ζ at about 225°C when photographs were taken at successive increasing temperatures i.e. when going from β' to ζ field, and ζ transforms to β' at about 220°C in the reverse process. But when the specimen was annealed in the camera for six hours before recording the pictures at every temperature, no such temperature hysteresis was observed. This revealed that $\beta'-\zeta$ transformation is not rapid and requires time to be completed. This phenomenon was also observed in the case of quenched alloys. An alloy, originally in the ζ state, when annealed at 220°C for two hours and quenched, gave ζ phase only, whose diffraction lines were not sharp but diffuse. This shows that the atoms of the ζ phase have started moving and are slightly displaced from the normal positions still-keeping the hexagonal symmetry i.e. the lattice is strained. However, the results obtained with the high temperature camera are that the alloy 51.3 is in the ζ phase at 230°C and in β' at 225°C. The mean value 227.5°C was accepted as the approximate transformation temperature for this alloy.

Powders of the 51.3 alloy were annealed at temperatures of 224°C, 227°C, 230°C and 234°C for five days and quenched in water and their diffraction photographs were taken. The results are that at 224°C the alloy is in the β' phase, at 227°C both β' and ζ are present, and at 230 and 234°C there is only the ζ phase. Hence 227°C was accepted as the transformation temperature.

The lattice parameter of the β' and ζ phases corresponding to all the four alloys were determined. The variation of the lattice parameter of β' phase with composition was rather small. No variation in the '*c*' parameter of the hexagonal ζ phase was observed and only the '*a*' parameter changed with composition. The lattice parameter of β' and ζ phases as well as the annealing temperatures are included in the Table II.

TABLE II

Lattice parameter of β' and ζ phases

β'			ζ				
Composition wt. % of Cd.	Annealing temp.°C.	Lattice parameter in Å	Composition wt. % of Cd.	Annealing temp. in °C	Parameter 'c' in Å	Parameter 'a' in Å	c/a
47.0	224	3.3314	47.0	235	4.8236	2.9835	1.617
50.8	224	3.3315	50.8	234	4.8240	2.9835	1.617
51.3	224	3.3316	51.3	235	4.8238	2.9840	1.616
51.57	224	3.3318	51.57	235	4.8238	2.9843	1.616
53.0	216	3.3323	53.0	226	4.8239	2.9854	1.615
56.4	215	3.3325	56.4	224	4.8238	2.9860	1.615
58.0	210	3.3326	58.0	230	4.8234	2.9862	1.614

The transformation temperatures of all the other alloys were established by examining the quenched powders. The results are given in the Table III. Alloy 53 when annealed for 15 days at 220°C, the accepted transformation temperature for this alloy, yielded both β' and ζ phases.

TABLE III

$\beta'-\zeta$ transformation temperatures

Composition of alloys; wt. % of cadmium	$\beta'-\zeta$ transformation temperature °C.	Phases
47.0	228	$(\alpha+\beta')-(\alpha+\zeta)$
50.8	228	$\beta'-\zeta$
51.3	227	,,
51.57	226	,,
53.0	222	,,
56.4	220	$(\beta'+\gamma)-(\zeta+\gamma)$
58.0	220	,,

An approximate value of thermal expansion for the β' and ζ phases were obtained from the high temperature photographs. For β' phase a value of 24×10^{-6} °C^{-1}, and for ζ phase values of $\alpha_c = 22\times10^{-6}$ °C^{-1} and $\alpha_a = 36\times10^{-6}$ °C^{-1} corresponding to the c and a axes respectively were obtained. The axial ratio c/a for the ζ phase changes from 1.617 to 1.614 with increasing cadmium concentrations. The value of c/a also decreases with increasing temperature.

The lattice parameter of β' and ζ phases were plotted against composition, and by extrapolation it was observed that the β' and ζ phases in 47% alloy correspond to 50.6 and 50.7% by weight of cadmium respectively. These gave the composition of the $(\alpha+\zeta)/\zeta$ and $(\alpha+\beta')/\beta'$ boundaries.

(iii) *The $\zeta/(\zeta+\gamma)$ and $\beta'/(\beta'+\gamma)$ phase boundaries*

The alloys 56.4 and 58% by weight of cadmium were studied by quenching method. A transformation temperature of 220°C$\pm$1 was obtained for both the alloys. The alloy 56.4 was also studied up to 400°C in the high temperature camera. The high temperature study of the alloy yielded 219°C$\pm$1 as the transformation temperature. The lattice parameters of the phases were calculated from the high angle lines. Lattice parameter of γ was 9.9704 Å for both the alloys. By extrapolating the lattice parameter for β' and ζ corresponding to these two alloys, the boundary between $\beta'/(\beta'+\gamma)$ and $\zeta/(\zeta+\gamma)$ was obtained. Alloys 47 and 56.4 were annealed for more than 15 days at 180°C and yielded an approximate boundary composition at that temperature. The results are included in the Table IV.

DISCUSSION OF RESULTS

The presence of the β' phase, which was suspected by Durrant and others from thermal and microscopical studies of the silver-cadmium alloys, has been confirmed by our X-ray investigation of the system. The β' phase boundaries determined by us are found to differ considerably from those given in Metals Handbook, these latter being based on the microscopical work of Durrant. The boundaries of the α and ζ phases obtained in the present work agree with those found by Owen *et al.* The boundary compositions of the different phases, as obtained in course of the present work along with those obtained by Owen, are given in Table IV. β'—ζ transformation temperatures of all the alloys examined are given in the Table III. These differ from those given in Metals Handbook by about 12°C.

TABLE IV

Boundaries in the silver-cadmium system of alloys

Temp.	Boundary composition (cadmium weight percent)							
°C.	$\alpha/(\alpha+\beta')$	$(\alpha+\beta')/\beta'$	$\beta'/(\beta'+\gamma)$	$\alpha/(\alpha+\zeta)$	$(\alpha+\zeta)/\zeta$	$\zeta/(\zeta+\gamma)$	$(\zeta+\gamma)/\gamma$	Author
180	43.3	50.6	53.6					1
215		50.6	53.65					1
224	43.4			43.5	50.7			1
235				43.5	50.7	53.75		1
250				43.5	50.75	54.0		2
270					50.75	54.0		2
300				43.6			59.6	2
210							59.6*	2
180							59.6*	2

1 Present work. 2 Owen, Roger and Guthrie (1939). *Corresponds to $(\beta'+\gamma)/\gamma$

With the help of these data the equilibrium diagram of the Ag-Cd system between the compositions of 40 to 60% by wt of cadmium and up to 300°C was constructed and is given in Fig. 1. The complete diagram of the system, shown in Fig. 2 was obtained by combining the results of Owen *et al.* with those of the present observations. This represents a complete diagram for the silver-cadmium system obtained from the X-ray study of the alloys in the solid state. However, the liquids and solids curves were not determined in the present investigation.

A duplex $(\beta'+\zeta)$ phase field is also included in the diagram, based on the observations on three alloys as mentioned earlier. It has not been possible to determine the extent of this duplex region precisely, but observations show that

it is confined within $\pm 2°C$ of the corresponding $(\beta' - \zeta)$ transformation temperature. The general arrangement of the phase fields is similar to that in the silver zinc

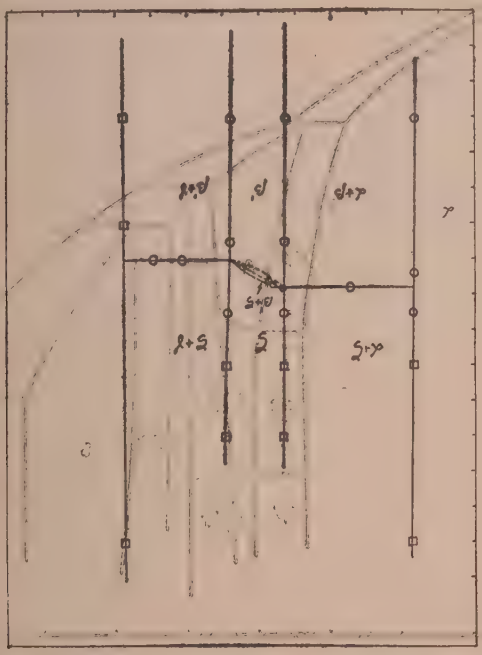

Fig. 1. Boundaries of the β'-phase in the Ag–Cd system.

system except that in the case of Ag-Zn there is only one $(\beta - \zeta)$ transformation at about 260°C, whereas in Ag-Cd system there are two transformations in the β-field.

The structures of the different phases in the diagram are : α phase, face-centred cubic; β phase, body-centred cubic; β' phase, ordered body-centred cubic with CsCl type of structure; γ phase, complex body-centred cubic with 52 atoms to the unit cell; and ζ, δ and ϵ phases are close- packed hexagonal. It is not possible to get evidence of long range order in β' phase from x-ray investigations in this case as the super-lattice lines cannot be recorded on account of the nearly equal scattering powers of silver and cadmium atoms. However, there is evidence from nuclear magnetic resonance experiments (Drain, 1959) that the silver and cadmium atoms strongly attract each other which shows that unlike atom pairs will be favoured in this alloy. It may be concluded that the β to ζ and again ζ to β' transformations are probably controlled by the order parameters and energy considerations.

The alloy 68% by weight of cadmium, which is in the δ phase field, was studied. The lattice parameters of the δ phase are: $a = 3.037$ Å $c = 4.824$ Å and $c/a = 1.588$.

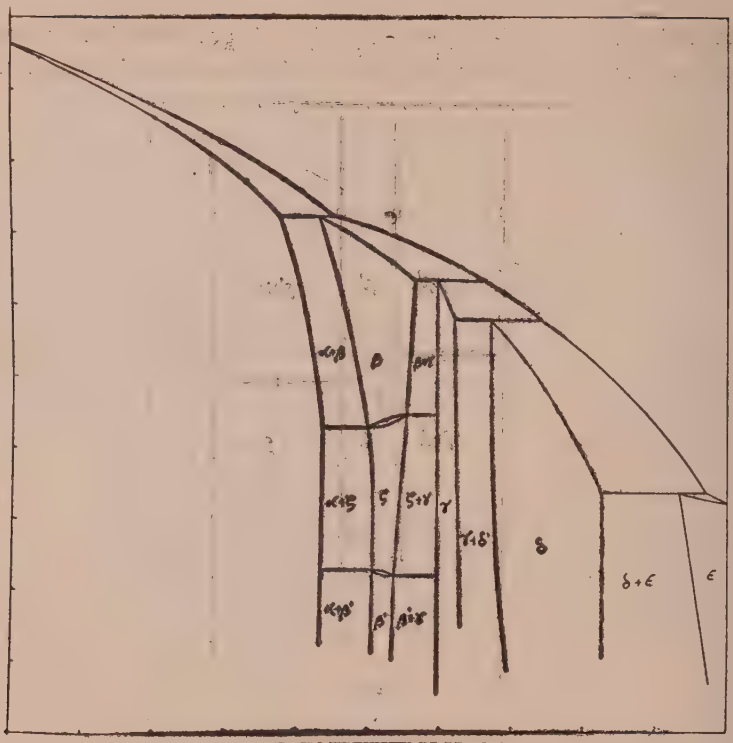

Fig. 2. Equilibrium diagram of silver-cadmium alloys based on the work of Owen *et al.*, and the present investigations.

The formation of the intermediate phases β, ζ and γ can be explained by the Hume-Rothery rule for electron compounds. Assuming that the electrons are nearly free and the Fermi energy is the most significant factor determining the stability of these phases, Jones (1934, 1937) has given a theoretical explanation of the Hume-Rothery rule from the zone theory of metals. According to this rule the α phase having f.c.c. structure should become unstable at the electron concentration 1.4 while from the equilibrium diagram (Fig. 1) of Ag-Cd alloys it comes out to be 1.425. Similarly for the $(\alpha+\beta')/\beta'$ boundary the Hume-Rothery rule gives 1.5 as against 1.496 found here. For the $\beta'/(\beta'+\gamma)$ and $(\beta'+\gamma)/\gamma$ boundaries we find the electron concentrations 1.528 and 1.586 as against 1.5 and 1.6 from the Hume-Rothery rule.

ACKNOWLEDGMENT

The author is indebted to Prof. B. N. Srivastava, D.Sc., F.N.I., for suggesting the problem and for his valuable guidance throughout the progress of this work.

REFERENCES

Astrand, H. and Westegren, A., 1928, *Z. anorg allgen chem.*, **175**, 90.
Drain, L. E., 1959, *Phil. Mag.*, **4**, 484.
Durrant, P. J., 1931, *J. Inst. Metals.*, **45**, 99.
Durrant, P. J., 1935, *J. Inst. Metals*, **56**, 155.
Jones, J., 1934, *Proc. Roy. Soc.*, **144**, 225.
Jones, H., 1937, *Proc. Phys. Soc.*, **49** 250.
Kosolapov, G. F., and Trapeznikov, A. K., 1936, *J. Tech. Phys.* (*USSR*), **6**, 1131.
Metals Handbooks, 1948, American Society for Metals.
Natta, G., and Freri, M., 1928, *Atti accad Lincei.*, **7**, 422.
Owen, E. A., Roger, J. and Guthrie, J. C., 1939, *J. Inst. Metals.*, **65**, 457.

57

IONIZATION OF E-LAYER BY X-RAYS

S. N. GHOSH AND SHARDA NAND

J. K. INSTITUTE OF APPLIED PHYSICS, UNIVERSITY OF ALLAHABAD, ALLAHABAD

(*Received, August* 16, 1960)

ABSTRACT. In this paper, the transmission curves for solar radiations in the X-ray and ultraviolet regions through the earth's atmosphere, obtained from rocket data and absorption coefficients have been utilized for determining the radiation responsible for E-layer ionization. It is found that only X-rays between the wavelength region 5 to 100A are absorbed in the region of the atmosphere occupied by E-layer. The amount of energy absorbed is 0.19 erg cm^{-2} sec^{-1}. The number of ions produced by (1) absorbed X-rays, (2) ejected photoelectrons produced by X-rays, and (3) Auger Effect induced by X-rays has been calculated and found to be 4×10^8, 5.6×10^9, and 2.5×10^8 cm^{-2} sec^{-1} $column^{-1}$ respectively or the total rate of production of ions in the E-layer is 6.2×10^9 cm^{-2} sec^{-1} $column^{-1}$. Remembering the error in the measurements of energy from a rocket, this value agrees with that obtained from substituting the value of effective recombination coefficient and electron density for E-layer in the expression $q = \alpha N_e^2$.

The temperature of the sun corresponding to different wavelength regions are calculated from data obtained from rocket-borne experiments. The calculated values agree with those given by Nicolet.

1. INTRODUCTION

E. O. Hulburt (1938) was the first to propose that soft X-rays may produce the *E*-region. Bates and Hoyle (1948) supported Hulbert's proposal. In considering auroral phenomena, Vegard (1923, 1938) also suggested that soft X-rays are a major contributor to the ionization at high altitudes. Also, from solar energy measurements by rocket-borne experiments, it appears that ionization of the *E*-layer is due to soft X-ray emissions from solar corona. Recently, Friedman (1959) suggested that *E*-region is produced by X-rays and Lyman-β (1025A), and D-region by Lyman-α (1216Å).

In this paper, the total amount of solar X-ray energy absorbed within the *E*-layer is calculated from the energy at the top of the earth's atmosphere obtained from rocket-borne experiments and the transmission curves for these radiations through the atmosphere. The rate of ionization produced by absorbed energy is then calculated and compared with other available value.

The temperatures of the sun at different spectral regions in the ultraviolet and X-rays are also calculated from the amounts of solar energy at the top of the earth's atmosphere, obtained from rocket-borne experiments.

2. TRANSMISSION CURVES FOR X-RAYS AND ULTRAVIOLET RADIATIONS

Fig. 1 shows the transmission of different wave-lengths through the earth's atmosphere. The solid curves (Friedman, 1959) represent the penetration of solar radiations into the atmosphere for vertical incidence obtained from rocket-borne experiments. The dot-dash curves (Byram *et al.*, 1954) show the penetration of certain radiations computed from absorption coefficients given by Compton and Allison (1953). Dotted line curves (Friedman *et al.*, 1951) represent the transmission of solar radiations observed from V-2 49 rocket using photon counters.

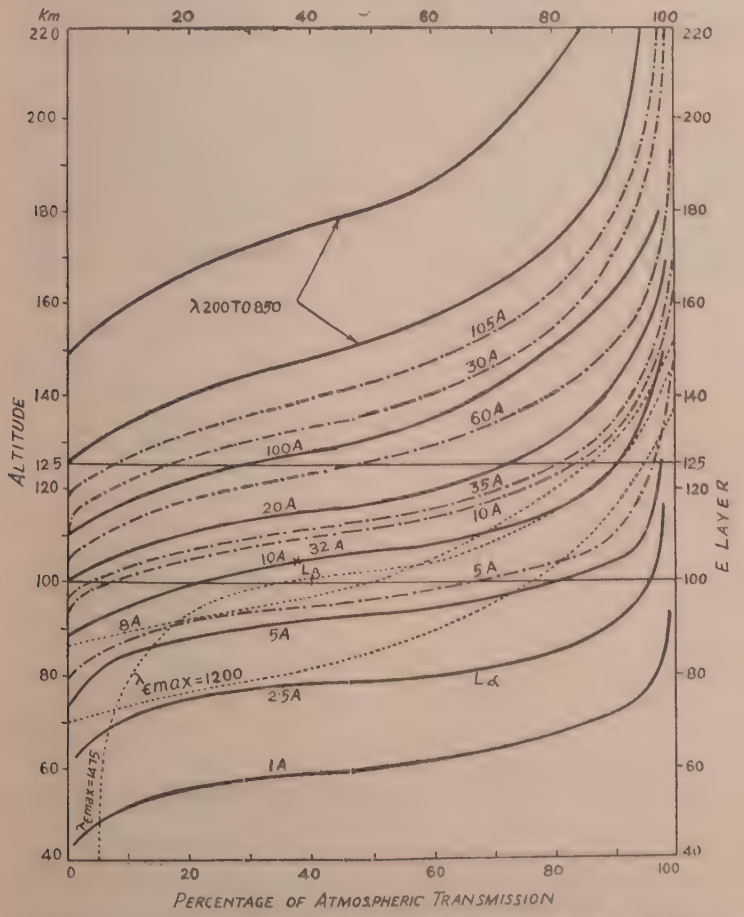

Fig. 1. Atmospheric transmission for different wavelengths in the X-ray and ultraviolet regions. The solid curves (Friedman, 1959) are obtained from rocket-borne experiments. Dotted line curves (Friedman, 1951) are also obtained using photon counters in V-2 49 rocket. Dot-dash curves are computed from absorption coefficients given by Compton and Allison.

It will be seen from above curves that, in general, radiations penetrate deeper into the atmosphere as the wavelength decreases. There are, however, certain departures. Wavelengths 1475A, Lyman-α, 1200A and Lyman-β penetrate much deeper into the earth's atmosphere. In the dot-dash curves, wavelength 30 A penetrated to a lesser depth compared to wavelengths 35A, 60A and 100A. Also, it may be noted that Lyman-α, and 2.5A, and wavelengths 10A and 32A have the same penetrating characteristics.

From the nature of these transmission curves, one can easily conclude that different amounts of energy corresponding to different wavelengths are absorbed at different altitudes of the atmosphere. Wavelengths from 200 A to 850 A are absorbed above 125Km, whereas those between 5A and 100A are absorbed in the region 90-125 Km. The Lyman-α radiation (Byram *et al.*, 1953) penetrates upto 74 $\pm$ 2 Km. Also, Lyman-β is absorbed between altitudes 90 and 125 Km. Wavelength 2.5A penetrates below 70 Km and 1A well below 60 Km.

From rocket data, 50 per cent transmission of energy at different wavelengths in the X-ray region is calculated and is shown in Fig. 2. The values given by Leo Goldberg (1954) for 50 per cent transmission of energy for higher wavelengths are also given in the same figure.

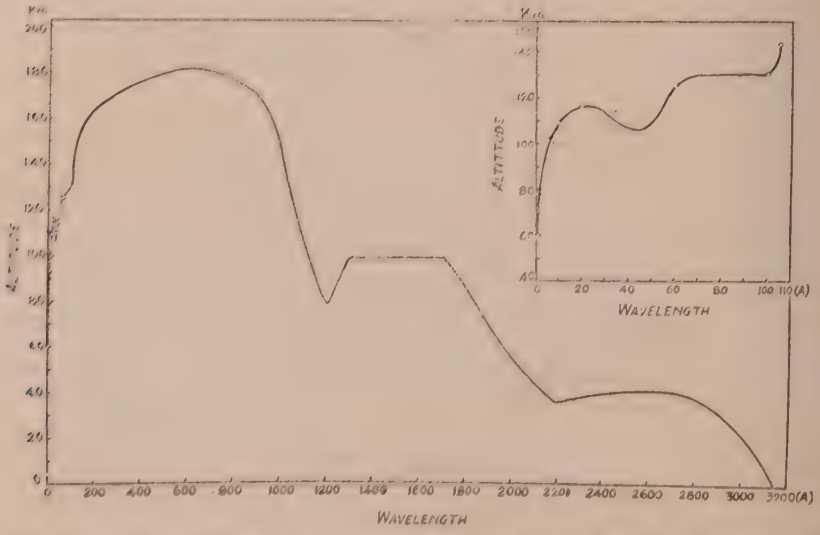

Fig. 2. Altitudes for 50 per cent transmission of solar energy in the X-ray region. Solid line curve is drawn by Leo Goldberg and the dashed curve (shown in a magnified scale on the right side) is obtained from the present work.

3. ABSORPTION OF X-RAYS IN E-LAYER

The results of measurements of electron density as obtained from different rocket flights at White Sands Proving Ground, New Mexico, are given in Table 1.

These measurements show that the height of the maximum ionization of the *E*-layer lies between 100 and 110 Km. It has also been observed that under normal conditions of the sun there is not much variation in electron density up to 125 Km, although during solar activity there is considerable variation. Therefore, for calculating the number of ion cm^{-2} sec^{-1} $column^{-1}$, the *E*-layer may be assumed to lie between 100 and 125 Km.

TABLE I

E-layer ionization from rocket data at white sands proving ground, New Mexico

Rocket flight, date and time	Authors	Altitude of maximum ionization Km	Remarks
May 7, 1947; 11-25 hrs. MST	*a*	About 110	Rapid increase in electron density from 85 Km to 110 Km; no measurement was made above 110 Km.
Jan. 22, 1948; 13-14 hrs. MST	*a*	100	Electron density increases from 92 Km to 100 Km. No data available above 100 Km.
V-2 No. 49, Sept. 29, 1949; 10-00 hrs. MST	*a*	107	Peak electron density at 107 Km. Between 110 and 125 Km, there is not much variation in electron density.
Viking No. 5, Nov. 21, 1950; 10.18 hrs. MST	*a*	110	Electron density gradient becomes steep from about 92 Km. Peak electron density is observed at 110 Km. There is not much variation in electron density between 110 and 125 Km.
Viking No. 10, May 7, 1954; 10-00 hrs. MST	*b*	Peaks at 101, 112 and 129	Measurements show a rapid increase in electron density at 91 and 101 Km.
Aerobee-38, June 26, 1953; 12.10 hrs. MST	*c*	110	A sharp maxima at 110 Km.
Aerobee-HI NRL-50, June 29, 1956; 12-09 hrs. MST	*d*	Sharp maxima at 101	Electron density increases from 92 to 160 Km. Between 100 and 125 Km, the electron density is practically constant.

a—Jackson, 1954 & Seddon, 1954 ; *b*—Seddon *et al.*, 1954 ; & Jackson, 1956 ; *c*—Pfister *et al.*, 1958 ; *d*—Jackson *et al.*, 1958.

Solar energy values at the top of the earth's atmosphere for different wavelengths were obtained from rocket flights and are shown in Section 5 (Table 4). The percentage of absorption of these radiations in the *E*-layer was calculated from Fig. 1. Assuming the *E*-layer to lie between altitudes 100-125 Km, the energy absorbed in this layer corresponding to different wavelengths is then calculated and is given in Table II. A graph is drawn between the absorbed energy and wavelengths and is shown in Fig. 3. The integrated area gives the total

amount of X-ray energy absorbed in the *E*-region. Its value is estimated to be 0.19 erg cm^{-2} sec^{-1}. [The Lyman-β (λ 1025) radiation is also absorbed between

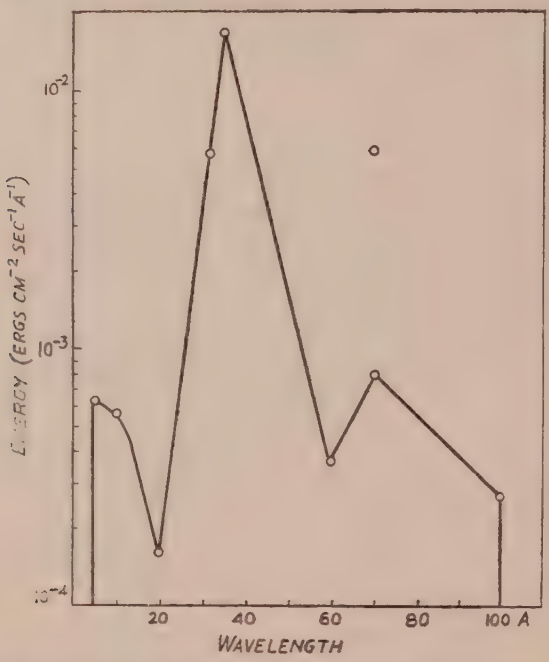

Fig. 3. The solar energy in the X-ray region absorbed in the E-layer as calculated from Fig. 1. The E-layer is assumed to lie between altitudes 100 and 125 Km. Corresponding to 70 Å two energy values, 2×10^{-3} and 1.5×10^{-2} ergs cm^{-2} sec^{-1} A^{-1} were obtained by Friedman (1959). In the present calculations only the lower value is taken.

the altitudes 100-125 Km. However,it does not produce *E*-layer ionization because it requires radiations of wavelength less than 1019A].

TABLE II

Solar energy in the X-ray region absorbed between altitudes 100 and 125 Km

Wavelength (A)	Percentage of energy absorbed	Energy absorbed (erg cm^{-2} sec^{-1} A^{-1})
5	25	6.25×10^{-4}
10	75	5.63×10^{-4}
20	75	1.62×10^{-4}
32	70	5.81×10^{-3}
35	85	1.70×10^{-2}
60	50	3.75×10^{-4}
70	40	8.00×10^{-4}
100	30	2.70×10^{-4}

4. IONIZATION IN E-LAYER BY X-RAYS

Assuming that X-rays absorbed in the E-layer are responsible for its ionization, the number of ions produced in this layer has been calculated as follows :

The amount of energy absorbed in the *E*-layer in an interval of 5Å has been obtained from Fig. 3. The mean photon energy in the interval is then calculated. Dividing the former by the latter gives the number of photons. Knowing the number of photons in the interval of 5A. the rate of production of ions* in the *E*-layer by X-rays emitted by the sun has been calculated.

The rate of production of O^+ ions. $q(O^+)$, will depend upon the product of absorption coefficient, α_0, of O atoms corresponding to frequency ν and its concentration, $n(O)$. Therefore,

$$q(O^+) \propto \alpha_0 n(O). \qquad \ldots \quad (1)$$

Similarly, in the case of nitrogen atoms

$$q(N^+) \propto \alpha_N n(N). \qquad \ldots \quad (2)$$

Therefore,

$$\frac{q(N^+)}{q(O^+)} = \frac{\alpha_N n(N)}{\alpha_0 n(O)} \qquad \ldots \quad (3)$$

or,
$$q(O^+) = \frac{\alpha_0 n(O)[q(O^+)+q(N^+)]}{\alpha_0 n(O)+\alpha_N n(N)} \qquad \ldots \quad (4)$$

Substituting A for $[q(O^+)+q(N^+)]$ which is the total rate of production of ions in the *E*-layer or the number of photons absorbed, the Eqn. (4) becomes

$$q(O^+) = \frac{\alpha_0 n(O)}{\alpha_0 n(O)+\alpha_N n(N)} \times A.$$

Similarly,
$$q(N^+) = \frac{\alpha_N n(N)}{\alpha_0 n(O)+\alpha_N n(N)} \times A.$$

The absorption coefficients of atomic oxygen and nitrogen have been taken after Compton and Allison (1953) and the particle concentration after Nicolet (1959). The ejected photoelectrons are loaded with excess energy and cause valence ionization of other atoms. Also, from Auger Effect for K-L shell transition for O and N atoms there exists 50 per cent probability of electron ejection and

* The photons corresponding to wavelengths $\leqslant$ 23.58 A and 31.18 A. eject K electrons from oxygen and nitrogen atoms respectively, while those corresponding to wavelengths greater than the above values eject L electrons.

50 per cent for X-ray emission. The rates of ion production by the above processes are given in Table III.

TABLE III

Ion production due to X-rays in the *E*-layer by different processes

Gas	K-shell ionization	L-shell ionization	Valence shell ionization	Ionization by Auger Effect	
				Direct electron ejection	From X-ray emission
	($cm^{-2}s^{-1}col^{-1}$)	($cm^{-2}s^{-1}col^{-1}$)	($cm^{-2}s^{-1}$ col^{-1})	($cm^{-2}s^{-1}$ col^{-1})	($cm^{-2}s^{-1}$ col^{-1})
Oxygen	2.5×10^{6}	1.6×10^{3}	2.2×10^{9}	1.2×10^{6}	2.4×10^{7}
Nitrogen	1.8×10^{7}	2.2×10^{8}	3.4×10^{9}	8.8×10^{6}	2.2×10^{8}
Total	2.0×10^{7}	3.8×10^{8}	5.6×10^{9}	1.0×10^{7}	2.4×10^{8}

Therefore, the average rate of ion production in the *E*-layer is 6.2×10^{9} cm^{-2} sec^{-1} $column^{-1}$.

Another value for the rate of production of ions can be obtained by substituting the values of α and Ne in the expression for the rate of production of ions at equilibrium condition, namely,

$$q = \alpha Ne^{2} \qquad \ldots \quad (5)$$

where,

q—rate of ion production,

α—effective recombination coefficient,

and Ne—ionization density.

The value of α as given by different investigators (Appleton, 1959 ; Landmark, 1956) ranges from 1×10^{-8} to 4×10^{-8} cm^{3} sec^{-1}. The calculated value of the rate of total ion production due to X-rays agrees with the value obtained from the expression (5) if $\alpha = 6\times10^{-8}$ cm^{3} sec^{-1} and $Ne = 2\times10^{5}$ cm^{-3}. It may, however, be noted that the transmission curves (Fig. 1) were plotted from the data obtained from rocket-borne experiments by using photon counters and thermoluminescent phosphor technique. These data are liable to be in error. The measurements with photographs and ion chambers give more accurate values for the energy (Friedman, 1959 ; Jager, 1959).

5. TEMPERATURE OF SUN IN X-RAY AND ULTRAVIOLET REGIONS

We have already seen in Section 3 that the energy values at the top of earth's atmosphere corresponding to different wavelengths from ultraviolet to X-rays are obtained from rocket-borne experiments. From these energy values and considering the sun as a black body radiator, the coronal temperatures corres-

ponding to the emission of X-rays and ultraviolet radiations have been computed following the method of Nicolet (1952) as follows.

If $\rho(\nu)$ be the density of radiation emitted by the sun, then from Planck's formula

$$\rho(\nu) = \frac{8\pi h\nu^3}{c^3}\left(e^{h\nu/kT}-1\right)^{-1},$$

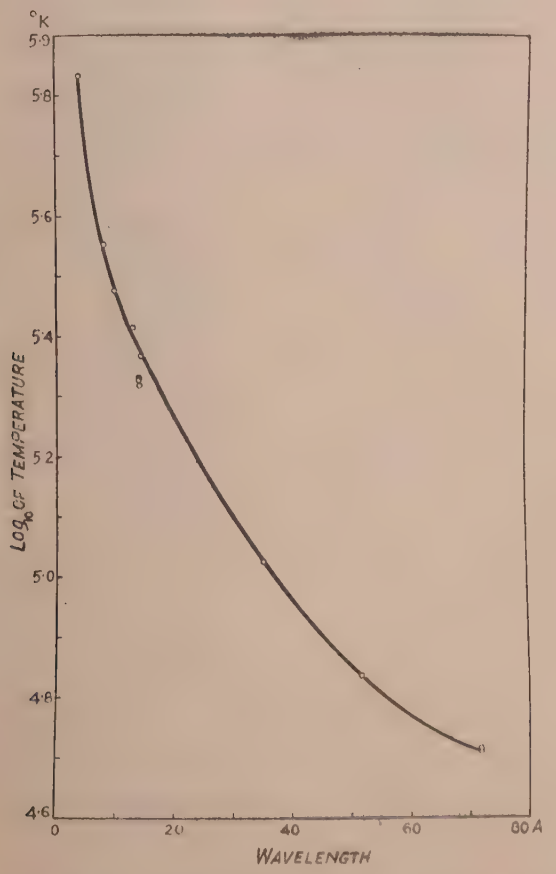

Fig. 4. Variation of temperature of the sun with wavelength in the X-ray region obtained from rocket data.

where the symbols have their usual significance. The radiation density $\rho'(\nu)$ at the top of the atmosphere is given by the relation

$$\rho'(\nu) = \beta_a \cdot \rho(\nu),$$

TABLE IV

Equivalent black body temperatures of the sun obtained from rocket-borne experiments in the X-ray and ultraviolet regions

Wavelength region (A)	Author	Condition of the sun	Energy (ergs cm^{-1} sec^{-1})	Equivalent black body temperature (°K)
Below 8	*a*	late in class I flare	5×10^{-3}	6.8×10^{5}
6 — 10	*b*	160 minutes after class I flare	$10^{-4}-10^{-3}$	3.5×10^{5}
8 — 12	*c*	quiet	3×10^{-3}	3.0×10^{5}
8 — 18	*d*	high coronal activity	0.6	2.6×10^{5}
8 — 20	*c*	–do–	0.1	2.3×10^{5}
8 — 20	*a*	quiet	1.5×10^{-3}	2.1×10^{5}
8 — 20	*a*	–do–	1.3×10^{-3}	2.1×10^{5}
8 — 20	*a*	–do–	1.2×10^{-3}	2.1×10^{5}
8 — 20	*a*	–do–	0.4×10^{-3}	2.1×10^{5}
10 — 60	*d*		1.0	1.1×10^{5}
44 — 60	*e*	minimum solar activity	1.4×10^{-2}	6.8×10^{4}
44 — 100	*e*	–do–	3.5×10^{-2}	5.2×10^{4}
44 — 100	*e*	–do–	2.9×10^{-2}	5.2×10^{4}
1050 — 1240	*f*	normal	0.4	5330
1200	*b*	–do–	6.2×10^{-2}	(6000)*
1216	*g*	no unusual solar activity	6.3	7730
1150 — 1340	*b*	–do–	1—10	5630
1230 — 1340	*b*	–do–	0.2	4840
1500	*b*	–do–	5.4×10^{-3}	(4500)*
2050	*h*	–do–	3.7	(5000)*

a — Chubb *et al.*, 1957 ; *b* — Friedman *et al.*, 1951
c — Burnight, 1952 ; *d* — Byram *et al.*, 1954 ;
e — Byram *et al.*, 1956 ; *f* — Tousey *et al.*, 1951.
g — Jager, 1959 & *h* — Byram *et al.*, 1952.

For figures marked with * the amounts of energy have been calculated from the given temperatures.

where the dilution coefficient β_s is given by

$$\beta_s = \frac{R^2}{4r^2} = \frac{(\text{sun radius})^2}{4(\text{sun-earth distance})^2}$$

$$= 5.41 \times 10^{-6}.$$

The temperatures thus calculated are given in Table 4. Comparing these values with the equivalent black body temperatures calculated by Nicolet (1952) from the coronal radiation of the quiet sun given in Table V, we find that there is a fair agreement between the two sets of values. The variation of temperature with wavelengths in the X-ray region is shown in Fig. 4. It may, however, be pointed out that the emission from the sun may be of grey body type (Byram *et al*, 1956). If such be the case, the actual temperature will be higher than those given in Table IV.

TABLE V

Equivalent black body temperatures of quiet sun in the X-ray and ultraviolet regions obtained by Nicolet

Wavelength (A)	Equivalent black body temperature (°K)
4	5.0×10^5
10	3.0×10^5
14	2.0×10^5
20	1.6×10^5
21.5	1.5×10^5
29.6	1.2×10^5
50	7.5×10^4
75	5.0×10^4
200	2.0×10^4
228	1.9×10^4
250	1.8×10^4
500	7.0×10^3
910	5.0×10^3
1000	5.0×10^3

REFERENCES

Appleton, E. V., 1959, *Proc. I.R.E.*, **47**, 155.

Burnight, T. R., 1952, Physics and Medicine of the Upper Atmosphere, pp. 233, University of New Mexico Press.

Byram, E. T., Chubb, T., Friedman, H., and Lichtman, S. W., 1952, *J. Opt. Soc. Amer.*, **42**, 876.

Byram, E. T., Chubb, T., Friedman, H. and Gailar, N., 1953, *Phys. Rev.*, **91**, 1278.

Byram, E. T., Chubb, T. and Friedman, H., 1954, Solar X-rays and E-layer Ionization, Rocket Exploration of the Upper Atmosphere, pp. 274, Pergamon Press Ltd., London.

Byram, E. T., Chubb, T. A. and Friedman, H., 1956, *J. Geophys. Res.*, **61**, 251.

Chubb, T. A., Friedman, H., Kreplin, R. W. and Kupperian, J. E. Jr., 1957, *J. Geophys. Res.*, **62**, 389.

Compton, A. H. and Allison, S. K., 1953, X-rays in Theory and Experiment, Macmillan and Co.

Friedman, H., Lichtman, S. W. and Byram, E. T., 1951, *Phys. Rev.*, **83**, 1025.

Friedman, H., 1959, Rocket Observations of the Ionosphere, *Proc. I.R.E.*, **47**, 272.

Goldberg, L., 1954, The Absorption Spectrum of the Atmosphere. The Earth as a Planet, Edited by G. P. Kuiper, pp. 434. The University of Chicago Press, Chicago, Illinois.

Hoyle, F. and Bates, D. R., 1948, *Terr. Mag.*, **53**, 51.

Hulburt, E. O., 1938, *Phys. Rev.*, **53**, 344.

Jackson, J. E., 1954, *J. Geophys. Res.*, **59**, 377.

Jackson, J. E., 1956, *J. Geophys. Res.*, **61**, 107.

Jackson, J. E. and Seddon, J. C., 1958, *J. Geophys. Res.*, **63**, 197.

Jager, C. D., 1959, Handbuch Der Physik, Published by Springer-Verlag, Berlin. Gottingen, Heidelberg.

Landmar, B., 1956, Solar Eclipses and the Ionosphere, Pergamon Press, London.

Nicolet, M., 1952, Annales de Geophysique, Tome 8, fascicule 2, 141.

Nicolet, M., 1952, Physics and Medicine of the Upper Atmosphere, pp. 201, University of New Mexico Press.

Nicolet, M., 1959, La Thermosphere, Annales de Geophysique, Tome 15, N° 1, 1–21.

Pfister, W. and Ulwick, J. C., 1958, *J. Geophys. Res.*, **63**, 315.

Seddon, J. C., 1954, *J. Geophys. Res.*, **59**, 463.

Seddon, J. C., Pickar, A. D. and Jackson, J. E., 1954, *J. Geophys. Res.*, **59**, 513.

Tousey, R., Watanabe, K. and Purcell, J. D., 1951, *Phys. Rev.*, **83**, 792.

Vegard, L., 1923, Skr. Vid. Selsk, I, Nos. 8, 9 and 10.

Vegard, L., 1938, *Geofys. Public.*, **12**, 23, 2pls.

58

ANALYSIS OF RANDOM FADING RECORDS

S. R. KHASTGIR

Calcutta University

AND

R. N. SINGH

Banaras Hindu University

(*Received, September* 3, 1960)

ABSTRACT. The analysis of the three-spaced-receiver fading records taken at Banaras from November, 1956 to March, 1958, with vertically-directed pulse transmission on 3.8 Mc/s has yielded the following results :

(*i*) The ratio of the drift velocity v_ω to the *r.m.s.* line-of-sight velocity v_o of the ionospheric irregularities is not found to be constant, as is expected from theory. The ratio increases with the increasing drift velocity.

(*ii*) The ratio of the drift velocity v_ω to the product of the frequency of fading N and the wavelength λ is not found to be constant, as is expected from theory. The ratio decreases with the increasing drift velocity.

(*iii*) The angle of spread of the scattered components from the ionospheric irregularities obtained from $\theta_o = \sin^{-1}(N \cdot \lambda/2v_\omega)$ is found to increase with the increasing drift velocity.

THEORETICAL CONSIDERATIONS

Ratcliffe (1948) developed a theory of the randomly fading radio waves. According to the theory, the irregularities in the ionosphere are the scattering centres which may be regarded as gas molecules under thermal agitation. The distribution of velocity (in one dimension) can then be expressed as:

$$P(v) = A \cdot \exp\left(-\frac{v^2}{{v_0}^2}\right) \qquad \ldots \quad (1)$$

where $\int_{-\infty}^{\infty} P(v)dv = 1$ and v_0 is the r.m.s. line-of sight velocity of the irregular scattering centres.

The frequency of the scattered components suffers a Döppler shift of frequency due to the line-of-sight velocity of the scattering centres. Considering the frequency-shift, $f - f_0$, the power-spectrum is given by

$$W(f) = B. \exp\left[-\frac{\lambda^2(f-f_0)^2}{8{v_0}^2}\right] \qquad \ldots \quad (2)$$

where λ is the wavelength of the wave.

The auto-correlation function of the fading pattern may be written as

$$P_h(\tau) = \frac{\overline{R(t) \cdot R(t+\tau)} - [\overline{R(t)}]^2}{[\overline{R(t)}]^2 - [\overline{R(t)}]^2} \quad \ldots (3)$$

where $R(t)$ and $R(t+\tau)$ are the amplitudes of the fading signals at instants t and $t+\tau$. Since the auto-correlation function is proportional to the Fourier transform of the distribution of power in the power spectrum, it can be shown

$$P_R(\tau) = C. \exp. \left[- \frac{16\pi^2 v_0^2 \tau^2}{\lambda^2} \right] \quad \ldots (4)$$

The theory can be tested by finding whether the auto-correlation function of the fading pattern obeys this law, and if it does, the magnitude of v_0 can be obtained from the value of τ, where $P_R(\tau)$ falls to e^{-1} in the auto-correlogram Thus

$$v_0 = \frac{\lambda}{4\pi\tau} \quad \ldots (5)$$

If the spatial auto-correlation of the fading pattern is plotted as a function of distance in one direction from a fixed origin, it is possible that it would fall in a smooth manner. Ratcliffe and Pawsey (1933), Pawsey (1935) had shown that the spatial auto-correlation function falls to about 0.8 in a distance of one wavelength. If now the irregular ionosphere producing this pattern were to move with a velocity v_ω, the diffraction produced on the ground would move with velocity $2v_\omega$. Therefore the spatial auto-correlation function would fall to about 0.8 in time $\lambda/2v_\omega$.

If now we assume the space and time auto-correlation to be similar (say, Gaussian), then the space auto-correlation function will fall to e^{-1} in time

$$\tau = \frac{0.8\lambda}{2v_\omega . e^{-1}} = \frac{2.2\lambda}{2v_\omega} \quad \ldots (6)$$

Then comparing the relations (5) and (6) we obtain

$$v_0 = \frac{v_\omega}{4.4\pi}$$

or $$v_\omega / v_0 \approx 14 \quad \ldots (7)$$

McNicol (1049) developed a quick method of determining the r.m.s. line-of-sight velocity v_0 by counting the number of maxima N of the fading pattern per sec. The approximate relation was given by

$$v_0 = \frac{N.\lambda}{5} \quad \ldots (8)$$

Considering (7) and (8) we have

$$v_\omega = 14 v_0 = 14 \frac{N.\lambda}{5} = 2.8 N.\lambda \quad \ldots \quad (9)$$

Further Briggs (1951) assuming that the horizontal movement of the reflecting layer to be the main cause of fading deduced the relation :

$$N = \frac{2 v_\omega}{\lambda} \sin \theta_0 \quad \ldots \quad (10)$$

where θ_0 is the semi-angle of the cone of the down-coming waves. It will be noticed that this relation is the same as the relation (9) given by McNicol except for the constants.

RESULTS OF THE ANALYSIS OF THE FADING RECORDS

A number of three-spaced-receiver fading records taken at Banaras from November 1956 to March 1958 with vertically-directed pulse-transmission on 3.8 Mc/s has been analysed. The cross-correlation method has given the drift velocity. The same sets of records have been used to find the r.m.s. line-of-sight velocity v_0 of the irregularities in the ionosphere by finding the time at which the auto-correlation function falls to a value e^{-1} and using relation (5). Table I shows the results of the analysis. The various values of the drift velocities have been arranged in groups of 0—10, 10–20, 20–30 metres/sec. and the averages of these have been estimated.

TABLE I

Frequency 3.8 Mc/Sec.

Drift velocity v_ω metres/sec.	r.m.s. line-of-sight velocity of the ionospheric irregularities v_0 metres/sec.	v_ω/v_0
12	1.23	9.75
26	2.46	10.60
37	2.70	13.70
48	3.20	15.00
56	3.40	16.40
67	3.50	19.00
78	4.10	19.00
86	4.60	18.60
	mean	15.25

It is evident from the data given in Table I that the ratio of the drift velocity v_ω to the r.m.s. line-of-sight velocity v_0 of the ionospheric irregularities varies with

the magnitude of the drift velocity, the ratio being smaller for the lower values of the drift velocity and larger for the higher values. Clearly the results show a departure from the theoretical relation (7).

The relation between the drift velocity v_ω and the frequency of fading N has also been found by analysing the random fading records. In Table II are given the values of the frequency of fading N and of the ratio of the drift velocity v_ω to $N.\lambda$ for the different groups of the drift velocity. It is clear that the ratio $v_\omega/N.\lambda$ decreases with the increase of the drift velocity. This variation is a departure from the theoretical relation (9). Using the relations (9) and (10), the angles of spread of the scattered components from the ionospheric irregularities for the various values of the drift velocity have been calculated. The calculated values of the spread angle are also entered in Table II. It is interesting to note that the spread angle increases with the increase of the drift velocity.

TABLE II

v_ω meters/sec.	60N in cycles/min	$v\omega/N\lambda$ =const.	$\theta_0 = \sin^{-1}\frac{N.\lambda}{2v_\omega}$
12	1.8	5.83	4° 50′
26	4.2	4.64	6° 19′
37	7.7	3.60	8° 2′
48	10.5	3.43	8° 20′
56	13.0	3.23	8° 55′
67	16.7	3.00	9° 35′
78	20.8	2.81	10° 23′
86	27.2	2.40	12° 7′
	mean	3.62	

It may be mentioned that the angle of spread of the scattered components is of the same order as that obtained by Briggs (1951) and Rao and Rao (1958). The values of the spread-angle are also in agreement with the values obtained by Briggs and Philips (1950) and by Khastgir and Singh (1960) from the three-spaced-receiver fading records.

REFERENCES

Briggs, B. H., 1951. *Proc. Phys. Soc.* (*Lond.*), **64***B*, 255.

Briggs, B. H. and Philips, G. J., 1950. *Proc. Phys. Soc.* (*Lond.*), **63***B*, 907.

Khastgir, S. R. and Singh, R. N., 1960. *Jour. Atmos and Terr. Physics*, **18**, Nos 2 and 3.

McNicol, R. E. W., 1949. *Proc. Inst. Elec. Engrs.* **96**, Part III, 517.

Pawsey, J. L., 1935. *Proc. Camb. Phil. Soc.*, **31**, 125.

Rao, B. R. and Rao, M. S., 1958, *Jour. Brit. IRE*, **18**, No. 8, 493.

Ratcliffe, J. A., 1948. *Nature*, **162**, 9.

Ratcliffe, J. A. and Pawsey, J. L., 1933. *Proc. Camb. Phil. Soc.*, **20**, 301.

Letters to the Editor

The Board of Editors will not hold itself responsible for opinions expressed in the letters published in this section. The notes containing reports of new work communicated for this section should not contain many figures and should not exceed 500 words in length. The contributions must reach the Assistant Editor not later than the 15th of the second month preceding that of the issue in which the letter is to appear. No proof will be sent to the authors.

16

LATITUDE DEPENDENCE OF NUCLEONIC INTENSITY DURING AUGUST 24 - SEPTEMBER 20, 1957

LEKH VIR AND P. S. GILL

GULMARG RESEARCH OBSERVATORY, GULMARG).

As early as 1933, Messerschmidt (1933) and Steinmaurer and Graziadei (1933) observed a decrease in cosmic ray intensity during a magnetic storm. However, Forbush (1937) incorporating Cheltenham and Huancayo data with that of Hafelekar obtained by Hess and Demmelmair (1937) established the world-wide character of the decrease in cosmic ray intensity with magnetic storm. Since then various reports of such decreases have appeared in literature.

Various methods for measuring the amplitude of the decreases have been adopted by different workers. In this note, we have followed the method suggested by McCracken and Johns (1959). According to it, where the correlation coefficient between any two sets of data R_1 and R_2 is greater than 0.8, the measure of relative amplitude is defined as $(\sigma_1/R_1)/(\sigma_2/R_2)$ where

$$\sigma_1 = \sqrt{\frac{1}{N-1}\Sigma(R_i-\bar{R}_i)^2} \quad \text{and} \quad \bar{R}_i = \frac{1}{N}\Sigma R_i$$

and R_i is the daily mean intensity.

During the period considered, a large Forbush type decrease in intensity occurred. Using the definition given above, and comparing daily mean data, the relative amplitude of the decrease in the intensity of nucleonic component of cosmic radiation for ten sea-level stations with respect to Huancayo data has been computed. The results are plotted in Fig. 1.

The striking feature of this decrease, as is obvious from the Fig. 1, is that the curve does not flatten out beyond the latitude knee. Instead the relative amplitude goes on increasing even up to 82.9°N. Also the relative amplitude is not symmetrical about the geomagnetic equator.

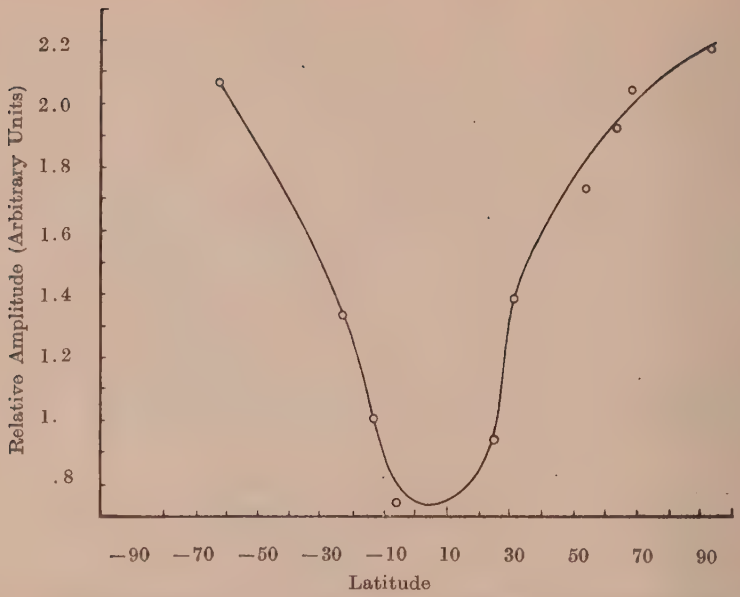

FIG. 1. Latitute dependence of a Forbush-type decrease. The relative amplitude is in arbitrary units.

REFERENCES

Forbush, S. E., 1937. *Phys. Rev.*, **51**, 1108.
Hess, V. F. and Demmelmair, A. 1937. *Nature*, **140**, 316.
McCracken K. G. and Johns, D. H., 1959. *Nuovo Cimento*, **13**, 96.
Messerschmidt, W., 1933. *Z. Phys.*, **85**, 332.
Stienmaurer, R., and Graziadei, H. T., 1933. *Akad. Wiss. Wien*, **22**, 672.

17

DEBYE Θ OF SOME CRYSTALS

S. K. JOSHI AND S. S. MITRA*

PHYSICS DEPARTMENT, ALLAHABAD UNIVERSITY, ALLAHABAD-2,

(*Received, June* 25, 1960)

Because of its inherent relationship with lattice vibrations, Debye characteristic temperature, Θ enters into a large number of solid state problems. The importance of this parameter and the scarcity of the available data have prompted us (Joshi and Mitra, 1960) to calculate and tabulate the Debye temperature of a large number of solids utilising the recent values of their elastic constants. In

* Now at Ontario Research Foundation, Canada,

TABLE I

Debye characteristic temperature and elastic constants for some crystals

(1) Cubic system

Formula	Substance	Elastic constants in unis of 10^{11} dynes/cm^2				Debye Temp. in °K	
		c_{11}	c_{44}	c_{12}	Source	Calculated	Exptl.
CsBr	Cesium bromide	3.097	0.7500	0.903	Reinitz and Huntington (1960)	136	
CsI	Cesium iodide	2.434	0.6316	0.636	Reinitz and Huntington (1960)	120	
Nb	Niobium	19.2	5.68	13.4	Bolef and Menes (1960)	283	
RbBr	Rubidium bromide	3.15	0.384	0.493	Reinitz and Huntington (1960)	127	
RbI	Rubidium iodide	2.54	0.276	0.407	Reinitz and Huntington (1960)	99	100–118
Ta	Tantalum	26.5	8.31	15.9	Bolef and Menes (1960)	259	246
V	Vanadium	22.9	4.38	11.7	Bolef and Menes (1960)	394	338

(2) Hexagonal system

Formula	Substance	Elastic constants in units of 10^{11} dynes/cm^2						Debye Temp. in °K	
		c_{11}	c_{33}	c_{44}	c_{22}	c_{13}	Source	Calculated	Exptl.
Cds	Cadmium sulphide	8.432	9.397	1.489	5.212	4.638	Bolef *et al* (1960)	214	

(3) Trigonal system

Formula	Substance	Elastic constants in units of 10^{11} dynes/cm^2							Debye Temp. in °K	
		c_{11}	c_{33}	c_{44}	c_{66}	cc_{13}	c_{14}	Source	Calculated	Exptl.
Bi	Bismuth	6.17	3.63	1.074	1.879	2.38	−0.699	Eckstein *et al.*, (1960)	107	117

* Now I.C.I. Fellow, University of Aberdeen.

the present communication it is intended to calculate the Debye Θ of some additional crystals belonging to the cubic, hexagonal and trigonal systems.

Only the lattice waves of nearly infinite wavelength contribute to the specific heat at very low temperatures, and Θ values derived from elastic constants are equal to those obtained from calorimetric data near 0°K. Θ is given by

$$\Theta = \frac{h}{k}\left(\frac{9N}{4\pi VI}\right)^{1/3}$$

where

$$I = \int_0^{4\pi} \sum_i \frac{1}{v_i^3} \frac{d\Omega}{4\pi}$$

h is Plack's constant, k is Boltzmann's constant, N is the number of vibrating units in volume V of the specimen and v_i are velocities of propagation for low frequency vibrations and as such are functions of direction. The subscript i numbers the solutions of the Christoffel equation for plane wave motion. It has been evaluated using Houston's series expansion method as modified by Betts *et al.* (1956).

For an accurate evaluation of Θ the values of elastic constants measured at about 0°K should be used (Alers and Neighbours, 1959). But in the absence of such data elastic constants measured at ordinary temperatures have been utilised, which yield an approximate value of Θ.

The values of Θ and the elastic constants from which they have been calculated for a number of substances belonging to the various symmetry classes are presented in Table I. The experimental Θ values derived from calorimetric measurements are also included, wherever available.

The authors are deeply indebted to Prof. K. Banerjee and Prof. S. N. Ghosh, for their interest in the investigation.

REFERENCES

Alers, G. A. and Neighbours, J. R., 1959, *Revs. Mod. Phys.*, **31**, 675.
Betts, D. D., Bhatia, A. B. and Wyman, M., 1956, *Phys. Rev.*, **104**, 37.
Betts, D. D., Bhatia, A. B. and Horton, G. K., 1956, *Phys. Rev.*, **104**, 43.
Bolef, D. I., Melamed, N. T. and Menes, M., 1960, *Bull. Am. Phys. Soc.*, **5**, 169.
Bolef, D. I. and Menes, M., 1960, *Bull. Am. Phys. Soc.*, **5**, 40.
Eckstein, Y., Lawson, A. W. and Reneker, D. H., 1960, *Bull. Am. Phys. Soc.*, **5**, 170.
Joshi, S. K. and Mitra, S. S., 1960, *Proc. Phys. Soc. (London)*, **76**, 295.
Reinitz, K. and Huntington, H. B., 1960, *Bull. Am. Phys. Soc.*, **5**, 40.

18

MAGNETISM OF THE IRON PARTICLES AS REVEALED BY ELECTRON DIFFRACTION

S. YAMAGUCHI

The Institute of Physical and Chemical Research, 31 Kamifuji (Hongo)
Tokyo, Japan

(*Received, September* 21, 1960)

The path of an electron beam is deflected in a magnetic field as the result of the Lorentz effect. This effect is observable in the diffraction pattern obtained from a ferromagnetic substance.

The rather soft electrons (about 50 KV) graze the surface of matter, whereas the hard electrons (about 200KV) are able to tunnel through a thick particle (thickness: about 3000 Å) (Yamaguchi, 1957, Yamaguchi and Takeuchi, 1957).

These two experiences imply that the alternative use of the soft and the hard electrons is of use for studying the surface magnetism of a given particle as compared with the interior magnetism of itself by means of diffraction.

Iron powder was here employed as a specimen for the experiment. The iron particles were magnetically attracted at the sharp edge of a razor blade acting as permanent magnet (remanence: about 10000 gauss). In this way these iron particles were kept in the saturation induction. An electron beam grazed these magnetized particles to give rise to a diffraction pattern.

A process of double exposure was carried in order to measure the Lorentz effect caused by the specimen. The diffraction pattern of a non-ferromagnetic gold foil was first photographed, and then that of the specimen was superimposed upon it. In this process, the position of the photographic plate as well as the wavelength of the incident beam were kept constant. Fig. 1 is a double diagram obtained in this process with the soft electrons (wavelength: 0.0479 Å). It is remarkable in this diagram that the diffraction rings from the reference gold foil and those of the specimen are eccentric as the result of the Lorentz effect. The ring eccentricity measurable in Fig. 1 makes it possible to calculate the magnetic induction at the surface of the specimen. Fig. 2 is a double diagram obtained with the hard electrons (wavelength : 0.0277 Å) from the same spot of the specimen as for Fig. 1. There is again the ring eccentricity in this diagram. This diagram informs us of the magnetic induction found in the interior of the particle specimen. We have a relation between Figs. 1 and 2 :

$$\frac{Z_1}{Z_2} = \frac{\lambda_1 B_s}{\lambda_2 B_i} \qquad \ldots \quad (1)$$

where Z_1 and Z_2 mean the ring eccentricity in Fig. 1 and that in Fig. 2, λ_1 and λ_2 mean the wavelength in Fig. 1 and that in Fig. 2 (0.0479 and 0.0277 Å), and B_s and B_i mean the surface and the interior inductions of the iron particles. From Figs. 1 and 2 we measure $Z_1 \; Z_2 = 1.59$. According to Eq. (1), therefore, we obtain

$$B_s/B_i = 0.92$$

or

$$B_s < B_i.$$

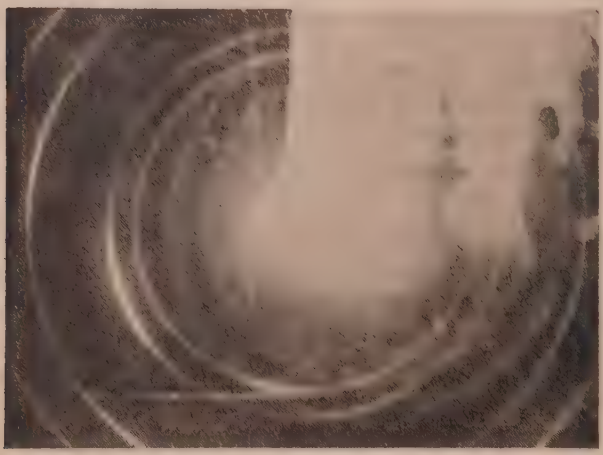

FIG. 1. A double diagram from the magnetized specimen and gold, taken with the soft electrons. Wavelength: 0.0479Å. Camera length: 495 mm. Positive enlarged 2.3 times.

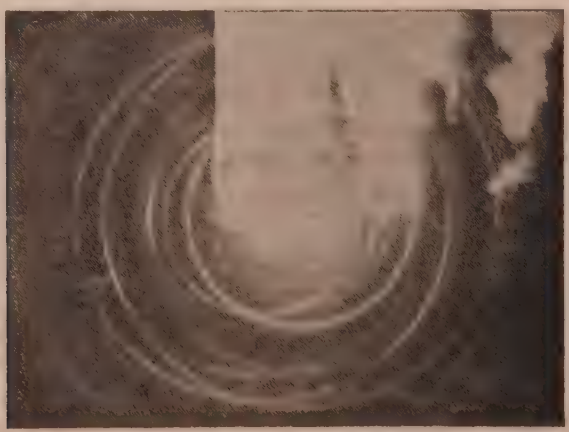

FIG. 2. A double diagram taken with the hard electrons. Wavelength: 0.0277Å.

The diffraction rings characteristic of the oxide (Fe_2O_4) in Fig. 1 with the soft electrons are distinctly more intense than those in Fig. 2 with the hard electrons. This fact verifies readily that the surface of the iron particles is covered with the oxide. The induction of this oxide is lower than that of pure iron. It is, therefore, reasonable for the present specimen that the surface induction B_s is lower than the interior induction B_i. A model of the iron particle under question is illustrated in Fig. 3.

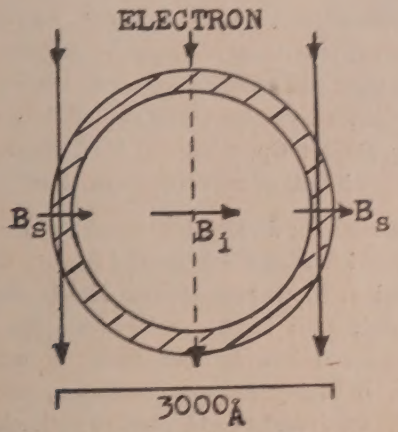

FIG. 3. The magnetic structure of the iron particle as revealed by electron diffraction. B_i and B_s mean the interior and the surface induction respectively.

REFERENCES

Yamaguchi, S. and Takeuchi, T., 1957, *J. Colloid Sci.*, **12**, 263.
Yamaguchi, S., 1957, *J. Chem. Phys.*, **27**, 1114.

BOOK REVIEW

FRONTIERS IN SCIENCE ; Edited by Edward Hutchings, Jr., pp.362+vi. George Allen Unwin Ltd, Ruskin House, Museum Street, London, 1960, Price 25 s. net.

Science is a continuous advance to new frontiers. Although, the geographic frontiers are disappearing, frontiers of Science are never ending. In the thirty-five most illuminating and exciting research reports that make up this volume frontiers of Science have been well explored by world renowned scientists like Linus Pauling, Robert Oppenheimer, Fred Hoyle, Sir Charles Darwin and twenty-eight other stalwarts of scientific researches.

The present volume has been divided into three main sections : the Physical Science, the Biological Sciences and Science and Society introduced respectively by George Beadle, Harrison Brown and Hunter Mead. Among many problems the interesting ones dealt with in this volume are the origin of life, growing population of the world and how to feed them, growth and reproduction of viruses, the structure of living matters, radiation, the life cycles of stars, natural disturbances, its cause and effects, place of technology in civilization and the relation of science and religion.

It is needless to mention that the present volume will be extremely helpful not only to scientists who are carrying on researches in the subjects discussed in this book, but also to non-scientists who want to keep themselves in contact with the current scientific developments.

The get-up of the volume is quite good.

(Dilip Kumar Ghosh)

CONTENTS

Indian Journal of Physics Vol. 34, No. 11 November, 1960

PRINTED BY KALIPADA MUKHERJEE, EKA PRESS, 204/1, B. T. ROAD, CALCUTTA-35
PUBLISHED BY THE REGISTRAR, INDIAN ASSOCIATION FOR THE CULTIVATION OF SCIENCE
2 & 3, LADY WILLINGDON ROAD, CALCUTTA-32